Solar Energy 301 (2025) 113984

Contents lists available at ScienceDirect

Solar Energy

journal homepage: www.elsevier.com/locate/solener

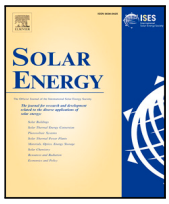

Robustness of cost-optimal energy system designs: The role of short-term extreme weather events and dispatchable generation

Wenxuan Hu [a,b,*], Yvonne Scholz [a], Madhura Yeligeti [a], Eugenio Salvador Arellano Ruiz [a], Patrick Jochem [a,b]

[a] German Aerospace Center (DLR), Institute of Networked Energy Systems, Curiestr. 4, 70563 Stuttgart, Germany
[b] Karlsruhe Institute of Technology (KIT), Institute for Industrial Production (IIP), Hertzstr. 16, 76187 Karlsruhe, Germany

ARTICLE INFO

Dataset link: https://zenodo.org/records/14983895, 10.5281/zenodo.14983895

Keywords:
Energy system model
Typical meteorological year
Synthetic weather year
Residual load
Extreme weather events

ABSTRACT

Modeling energy systems typically requires multiple weather years to ensure accurate results. However, running large-scale energy system models with multiple weather years is computationally intensive. To address this, a typical meteorological year is often used, which represents the long-term characteristics of historical weather. However, relying solely on such a representative year is insufficient due to the growing frequency of extreme weather events. It is crucial to consider how energy systems perform under extreme conditions to ensure a secure supply. This study addresses this need by focusing on weather-related extreme conditions of energy systems and employing various methods to generate synthetic weather years for a sector-coupled energy system. By configuring two system scenarios, we aim to identify a robust energy system configuration capable of accommodating all historical years. Additionally, we examine the characteristics of this system configuration and identify critical factors that influence system robustness to weather variability. Our results demonstrate the important role of dispatchable generation technologies in maintaining the security of supply. Furthermore, we find that short-term extreme events, such as 17 or 18 consecutive hours of extremely high residual load, can impose significant stress on the energy system, often exceeding the impact of longer-term extreme events.

1. Introduction

With the escalating challenge of climate change worldwide, the need to transition from fossil fuels to renewable energy sources has become increasingly urgent. However, the growing complexity of energy systems driven by the stochastic nature of fluctuating wind and solar generation and the increasing electrification of energy demand underlines the importance of robust energy systems [1]. To understand, analyze, and optimize modern energy systems, energy system models serve as a key tool. These models are mathematical representations of the complex interactions between energy demand, energy supply, conversion technologies, transmission networks, and other relevant factors [1,2]. By employing mathematical algorithms and optimization techniques, energy system models can capture the factors influencing energy supply and demand dynamics. They are crucial for policymakers, energy planners, and stakeholders to generate a range of insights and analyses of future energy systems developments [3].

The implementation of energy system models requires, among others, weather data as input. For example, hourly meteorological data on regional granularity, covering at least all four seasons of a year, is commonly applied. However, each year presents unique conditions. To accurately calculate the long-term average performance of the system, it is important to have a sufficient dataset covering multiple years and a suitable method for selecting the relevant patterns. Given the interannual variability and high granularity of meteorological data, such as wind and solar data, many studies incorporate data from several years to capture this variability and ensure robust system performance across different conditions. This approach, however, makes the modeling process cumbersome, time-consuming, and significantly increases model complexity [4–6]. As a result, synthetic, representative weather years are often generated.

The concept of representative weather years is widely used across various fields. Besides large-scale energy system analysis, it is also applied to building energy and performance simulations [7,8], evaluations of building-integrated photovoltaic (PV) systems [9], and other fields assessing crop yield and agricultural process studies [10–12]. Generally, representative weather years can be generated using various methods and are often referred to as example years, typical meteorological years (TMYs), or synthetic weather years (SWYs).

For example, a TMY is defined as a collection of weather data that is considered representative of average conditions, selected based on

* Corresponding author at: German Aerospace Center (DLR), Institute of Networked Energy Systems, Curiestr. 4, 70563 Stuttgart, Germany.
E-mail address: wenxuan.hu@student.kit.edu (W. Hu).

https://doi.org/10.1016/j.solener.2025.113984
Received 14 April 2025; Received in revised form 24 July 2025; Accepted 8 September 2025
Available online 17 September 2025

Abbreviation	Definition
CC	Correlation Coefficient
CDF	Cumulative Distribution Function
CF	Capacity Factor
CH4	Methane
CHP	Combined Heat and Power
EHY	Extreme High Residual Load Year
ELY	Extreme Low Residual Load Year
ESOM	Energy System Optimization Model
ExCCGT	Backpressure Combined Cycle Gas Turbine with Heat Extraction
FS	Finkelstein–Schafer
GT	Gas Turbine
H2	Hydrogen
PV	Photovoltaics
RE	Renewable Energy
SWY	Synthetic Weather Years
TMY	Typical Meteorological Year
VRE	Variable Renewable Energy

specific criteria [13]. The first effort to generate a TMY was undertaken by Hall et al. [14], resulting in the widely used Sandia method, named after Sandia National Laboratories. This method selects 12 typical months from historical data to form a TMY by comparing the long-term cumulative distribution function (CDF) with individual months using Finkelstein–Schafer (FS) statistics. The month with the smallest CDF differences is selected as the typical month. The method considers nine weather indices, including indices related to dry bulb and dew point temperatures, wind speeds, and solar radiation. By assigning weighting factors to each weather index, the TMY computation accounts for the monthly mean, median, and persistence of weather patterns.

In addition to the Sandia method, other researchers have explored different approaches. For example, Ratto and Festa [15] applied more comprehensive statistical indicators to estimate deviations of short-term CDF from long-term CDF using three standardized magnitudes. Gazela and Mathioulakis [16] introduced a more system-oriented method by emphasizing the monthly solar gains from multiple years of operation of a solar hot water system and the average solar gains. Additionally, the Chinese Meteorological Association proposed a method that uses normalized monthly mean values, calculated by subtracting the mean and dividing by the standard deviation, as selection criteria. The typical month with the least variability over a specific period is chosen [17].

Besides these deterministic approaches, stochastic methods that incorporate randomness and probability to generate multiple sequences of weather data have also been widely studied. These approaches account for the inherent uncertainty in weather inputs. Methods such as Autoregressive (AR) models [18–20], Markov Chain [21–23], Autoregressive Integrated Moving Average (ARIMA) models [24–26], and Vector Autoregressive (VAR) models [27–29] have been widely used for short-term weather data generation.

However, most studies primarily focus on identifying a representative weather year that captures average weather conditions. Given the increasing frequency and intensity of extreme weather events such as calm winds or dark doldrums ('Dunkelflauten') [30], it is crucial for energy system models to capture extreme weather events through the use of 'synthetic extreme weather years'.

For example, the Design Summer Year (DSY) is defined as a year positioned at the median of the upper quartile of historical datasets [31] or as the third hottest summer year [32]. This method ranks historical years based on the average dry-bulb temperature during the summer months. A variant of the DSY, the Probabilistic Design Summer Year, selects years using different metrics instead of average dry-bulb temperature [33,34]. Another approach involves adjusting the TMY through polynomial regression to adjust parameters such as dry-bulb temperature, global horizontal radiation, wet-bulb temperature, and wind speed, thereby generating a summer reference year [35,36]. Other methods include the Extreme Meteorological Year, which combines months with the highest and lowest hourly average values from all historical years to form a year with the hottest summer and coldest winter [37,38]. Recent methods include quantile regression aggregate summer years [39], extremely warm and cold years for building hydrothermal simulations [40], and extremely hot and cold reference years [41].

Additionally, some studies focus on selecting representative months or years by characterizing extreme weather events. For instance, Guo et al. [42] proposed three different years to characterize heat wave events, defining heat waves as temperatures exceeding 31.5 °C indoors and 35 °C outdoors. They introduced Typical Hot Years-Intensity, which identifies the year with the highest annual total heat event intensity based on simulated indoor dry-bulb temperature, emphasizing the intensity of extreme events. They also defined Typical Hot Years-Nights as the year with the greatest number of hot nights and Typical Hot Years-Events as the year with the highest combined event intensity and duration, both determined using simulated indoor dry-bulb temperatures. Similarly, Li et al. [43] used thresholds between the 5th to the 95th percentile to consider both the intensity and duration of extreme events, selecting representative extreme months based on this ranking.

However, these advanced studies have largely focused on meteorological aspects, particularly temperature extremes, without addressing the impact of extreme weather on energy systems, where factors such as residual load play more important roles. The definition of residual load varies across studies, it is generally defined as the total electricity demand minus the feed-in from variable renewable sources [44–46]. Research on residual load provides an estimation of the dispatchable power capacity required to meet electricity demand, which is particularly important given the inter-annual variability of solar PV and wind resources in highly renewable energy systems [46]. For example, Ohba et al. [47] explored the correlation between high residual load events and weather patterns, such as enhanced cold surge-type weather patterns during winter in Japan. Scholz et al. [48] used rolling averages of residual load anomalies, calculated as residual load minus its mean, to identify three types of extreme weather events: Dunkelflaute, seasonal electricity shortages, and long-term electricity shortages. Nitsch et al. [49] ranked extreme residual load events across historical years by categorizing them into durations of 1 day, 7 days, 14 days, and up to 365 days. Their analysis identified the winter of 1997 as the extreme period for various durations. Similarly, Höltinger et al. [50] investigated positive residual load events in Sweden lasting less than 4 h, 5–12 h, and 13–24 h, finding that the climatic conditions of 1987, 1996, and 2010 resulted in the highest number of extreme residual load events among the 29 investigated years. These studies have examined the characteristics of residual load, such as its frequency, duration, and intensity, establishing the strong correlation between high residual load events and extreme weather events. However, little effort has been devoted to generating synthetic weather years specifically designed to capture extreme residual load conditions. Addressing this gap requires generating synthetic extreme weather years that reflect highly positive residual loads and assessing their impacts on energy systems.

In this paper, we propose several methods to generate synthetic extreme weather years that capture critical residual load conditions for energy systems. These synthetic extreme weather years are then used as inputs for an energy system model to evaluate their impacts on system design and operation. Our ultimate goal is to identify a representative weather year for which an energy system designed based on this year can withstand and accommodate all investigated historical weather years. By assessing two energy system setting scenarios – exogenous and endogenous renewable capacity expansion – and investigating the key factors that influence the security of energy supply, we aim to

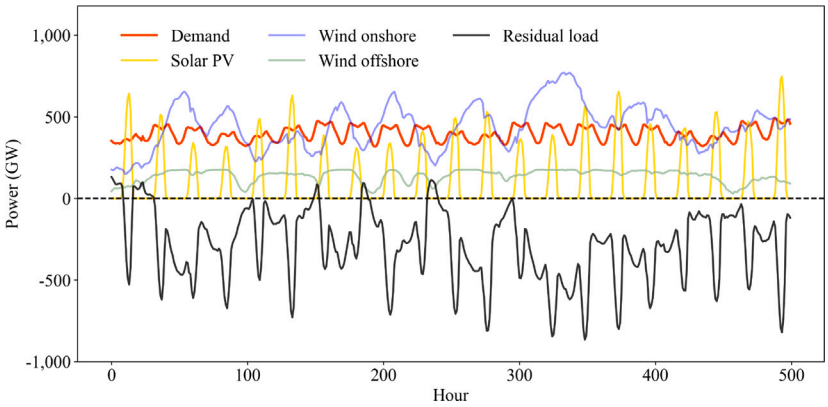

Fig. 1. The residual load, electricity demand, solar PV, wind onshore and offshore generation time series in the year 2020 for all study countries aggregated. For better visualization, only the first 500 h are displayed.

provide valuable insights into coping with possible future extreme weather events for energy system modelers.

This paper is organized as follows: Section 2 introduces the dataset and the energy system model used in this study. Section 3 describes the methods employed to identify and generate synthetic extreme weather years, along with the model scope description for two energy system configuration scenarios and system robustness evaluation. In Section 4, we provide a comparative analysis of the results, examining the impacts of different synthetic extreme weather years on the energy system model. Section 5 discusses the findings and the limitations of this study. Finally, Section 6 concludes with a summary of the results and key insights.

2. Data and model

2.1. Electricity demand time series

To generate electricity demand time series data, we apply the bottom-up approach described in [51]. This method employs national energy balances derived from the 'Distributed Energy' scenario from the Ten-Year Network Development Plan (TYNDP) 2022 [52], and focuses on fixed demands for electrical appliances, mobility services, and industrial processes. By using standard load profiles and time series data, this method can estimate electricity demand across various sectors while accounting for regional variations. The method has been calibrated with regional data and validated on an hourly basis against historical consumption patterns. The demand time series data are generated for a 30-year historical period spanning from 1991 to 2020.

2.2. Renewable energy generation time series

The renewable energy potential time series is generated using the global Energy Data Analysis Tool (EnDAT) [53,54]. The time series also covers 30 historical years from 1991 to 2020. The process begins with an area analysis in EnDAT, where exclusion zones and area competition criteria are applied. Geographic constraints such as land cover, distance from settlements, elevation, protected areas, and others are considered alongside area suitability factors to assess the area potential for renewable energy generation. Wind speeds, solar irradiance, and temperatures are extracted for the identified areas from meteorological datasets. In our case, the database is the global ERA5 reanalysis data set by the European Centre for Medium-Range Weather Forecasts (ECMWF) [55], which offers a spatial resolution of approximately 31 km × 31 km. Finally, power plant models of wind and PV plants are applied to calculate the capacities that can potentially be installed and the corresponding power generation time series. The data are initially calculated for each grid cell and then spatially aggregated to obtain renewable energy potentials at the national level.

To fit the renewable generation time series and demand time series to our system set-up, we scale them based on the renewable capacity values and demand value derived from the FlexMex[1] scenario 4D [56, 57], which assumes endogenous capacities of flexibility options and a Variable Renewable Energy (VRE) penetration of 160% of annual electricity demand[2] as the assumption [56]. This scaling results in hourly solar PV, onshore wind, offshore wind, daily run-of-river generation, and hourly demand profiles.

Residual load, defined as the difference between electricity demand and non-dispatchable power generation,[3] is a key metric in this study. A positive residual load indicates that demand exceeds power generation by non-dispatchable units, suggesting a potential electricity shortfall, while a negative residual load indicates surplus generation. Fig. 1 presents the input demand, solar PV, onshore wind, offshore wind generation, and residual load time series for all study countries aggregated in the year 2020. To ensure consistency and comparability across all years, all time series in this study are standardized to 8760 hours per year, with February 29th removed from leap years in the analysis.

2.3. Energy system model

To investigate the impact of different weather years on the energy system, we use the Energy System Optimization Model (ESOM) with the framework of REMix [58]. REMix is an open-source tool developed for identifying cost-optimal energy systems under various constraints. In this study, the model is configured to optimize system capacities and operations over a one-year period with hourly resolution, with the objective of minimizing overall system costs. The model optimizes generation and storage capacities individually for each country, while also incorporating cross-border grid interconnections to capture regional interactions and power exchange.

Besides the time series input data, other technological data used in this study are also derived from the FlexMex model experiment dataset. The time horizon of our model is set to 2050, and it considers

[1] FlexMex is a model experiment dataset (grant number: 03ET4077A-H), funded by the German Federal Ministry for Economic Affairs and Energy (BMWi) [56,57]. This publicly available dataset contains harmonized exogenous parameters, such as plant capacities, techno-economic factors, and heat demand, across 16 distinct test scenarios. These scenarios differ in terms of renewable energy capacity, the inclusion of endogenous capacity expansion options for flexibility, and the scope of technological components considered in the system [56].

[2] We choose 160% VRE penetration to compensate for VRE losses and curtailment.

[3] Run-of-river generation is excluded from the residual load calculation due to an assumed constant time series across all weather years and its relatively small contribution compared to other renewable technologies.

Table 1
Overview of the duration, intensity, and final scores for each historical year.

Year	Duration score	Intensity score	Final score	Year	Duration score	Intensity score	Final score
1991	0.784	0.642	0.713	2006	0.728	0.686	0.707
1992	0.507	0.469	0.488	2007	0.440	0.308	0.374
1993	0.456	0.590	0.523	2008	0.000	0.000	0.000
1994	0.416	0.344	0.380	2009	0.355	0.341	0.348
1995	0.472	0.235	0.354	2010	0.533	0.335	0.434
1996	0.592	0.459	0.525	2011	0.499	0.381	0.440
1997	1.000	1.000	1.000	2012	0.480	0.502	0.491
1998	0.104	0.199	0.152	2013	0.435	0.378	0.406
1999	0.131	0.044	0.088	2014	0.523	0.427	0.475
2000	0.373	0.437	0.405	2015	0.184	0.388	0.286
2001	0.392	0.457	0.424	2016	0.573	0.447	0.510
2002	0.680	0.695	0.687	2017	0.336	0.560	0.448
2003	0.549	0.532	0.541	2018	0.312	0.183	0.247
2004	0.672	0.637	0.655	2019	0.035	0.008	0.021
2005	0.131	0.075	0.103	2020	0.269	0.214	0.242

11 countries in Central Europe, corresponding to 11 model regions: Austria, Belgium, Denmark, Czech Republic, France, Germany, Italy, Luxembourg, the Netherlands, Poland, and Switzerland. The scope of the study includes a variety of technologies across different categories. For energy generation, the model includes PV, Onshore and Offshore Wind Turbines, Hydropower with Reservoir Storage and Run-of-River Hydropower. Gas-driven thermal power plants are split into two technology groups: Combined Heat and Power-Backpressure Combined Cycle Gas Turbines with Heat Extraction (CHP-ExCCGT) and Methane Gas Turbines (CH4-GT) for power production alone. Energy storage technologies considered in the model include Lithium-Ion Batteries, Hydrogen (H2) Caverns, Hydrogen Tanks, Thermal Storage, along with Pumped Hydro storage. Heating technologies, such as District Heating with CHP-ExCCGT, Heat Pumps, Gas Boilers, and Electric Boilers are also included. Additionally, the model also accounts for Electric Vehicles (EVs) with uncontrolled charging and decentralized Hydrogen Electrolysis with flexible hydrogen production. Power transmission is modeled with an aggregated representation of the high-voltage electricity transmission network within the model scope. The model optimizes transmission capacities and power flows based on cost estimates from the Ten-Year Network Development Plan (TYNDP) [59].

3. Methods

In this section, we describe the methodology applied to generate different synthetic extreme weather years and the model scopes for two different system setting scenarios and for evaluating the system robustness.

3.1. Generation of extreme weather years

3.1.1. Intensity and duration score

The first method we apply is identifying the most extreme weather years from the historical data. This process starts with establishing a ranking system to assess the extremity of each year, similar to [43]. The residual load time series are first aggregated across all 11 study countries before the analysis, enabling the examination of extreme conditions on a large scale. We define an extreme condition as a residual load exceeding the 95th percentile of all hourly historical residual loads, which corresponds to approximately 153 GW. The 'extreme periods' are any intervals where this threshold is exceeded. To quantify the extremity of each year, we assess both the intensity and the duration of these extreme periods. While the duration is defined as the number of consecutive hours in which the residual load exceeds the 95th percentile threshold, the calculation of the intensity of extreme periods is described in Eq. (1).

$$\mathrm{Int} = \sum_{i}^{\mathrm{Dur}} \left(\mathrm{R}_i - \mathrm{T}\right) \tag{1}$$

where,

- Int = Intensity of an extreme weather event
- Dur = Duration of an extreme event
- R_i = The residual load at the hour i
- T = Threshold for the extreme period, in this study, T is set to the 95th percentile of all historical residual load

Once the intensity and duration of extreme periods are calculated, each candidate year is ranked according to these two dimensions. To select the most extreme year, we assign equal weight to both duration and intensity, combining them to calculate a final score for each year. The year with the highest final score is chosen as the representative extreme historical year. Before calculating the final score, the duration and intensity values are normalized to a scale of 0 to 1 to ensure uniformity across all metrics.

Table 1 presents the intensity, duration, and final scores for each historical year. From this table, we can see that 1997 appears to be the most extreme year, both in terms of the intensity and duration of the events. Besides 1997, other relatively extreme historical years include 1991, 2006, 2002, and 2004.

3.1.2. Finkelstein–Schafer statistics method

The Finkelstein–Schafer (FS) statistic is a widely used method for measuring the distance between two cumulative distribution functions (CDFs) and is frequently used in the Sandia method. The Sandia method evaluates nine critical climatic indices, including daily maximum, minimum, and mean dry bulb and dew point temperatures, daily maximum and mean wind speeds, and daily total horizontal solar radiation. In this study, however, we focus exclusively on the residual load time series.

The core concept of the method involves selecting 12 representative months, which are then aggregated to construct a representative year. The selection of each representative month is based on the calculated distance between the CDF of that month in each historical year, referred to as the short-term CDF, and the CDF of all 30 historical years, referred to as the long-term CDF. This distance is measured using the FS statistic, as defined in Eq. (2). In the Sandia method, which aims at generating the TMY, the month with the smallest absolute FS value, indicating the closest match between the short-term and long-term CDFs, is selected as the representative month. However, our study, which aims to identify a representative extreme year that captures the critical conditions for the energy system, adopts a different approach. In addition to selecting months with the smallest absolute FS values, we also identify months with the highest positive and negative FS values. These correspond to months with extremely high and low overall residual loads, respectively, as illustrated in Fig. 2, which presents examples of both long-term and short-term CDFs for January. This approach allows us to generate three synthetic weather years:

- TMY: Typical Meteorological Year, representing historical average residual load conditions.

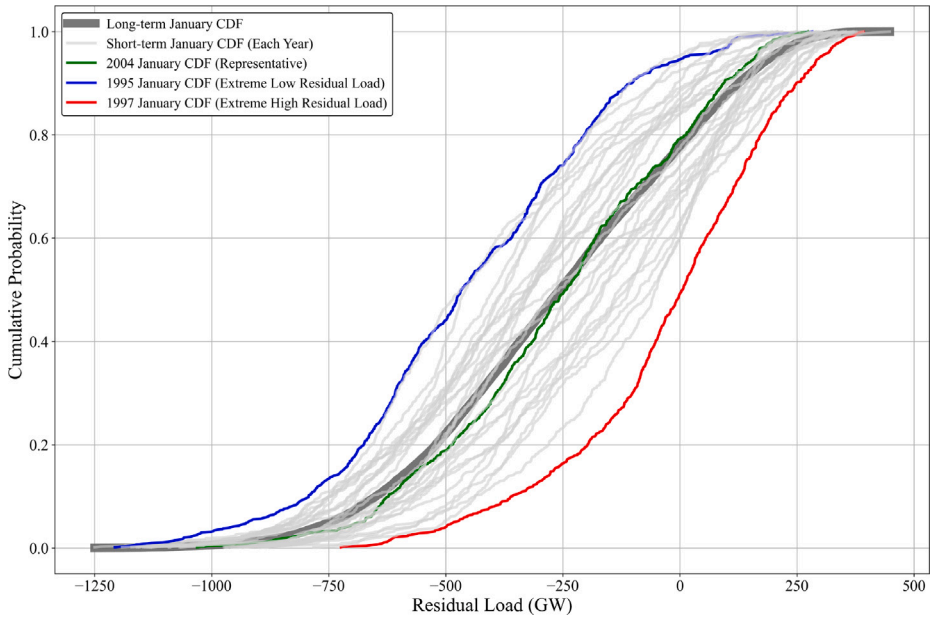

Fig. 2. Long-term and short-term CDFs for January. By calculating the distances between long-term and short-term CDFs using FS statistics, January 2004 is identified as the typical representative month due to its smallest absolute FS statistic. In contrast, January 1997 and January 1995 are identified as representative extreme months, with January 1997 representing a high residual load month and January 1995 representing a low residual load month.

- ELY: Extreme Low Residual Load Year, representing overall low residual load.
- EHY: Extreme High Residual Load Year, representing overall high residual load.

$$\mathrm{FS}(y,m) = \frac{1}{N}\sum_{i=1}^{N}\left|\mathrm{CDF}_m(x_i) - \mathrm{CDF}_{y,m}(x_i)\right| \tag{2}$$

where,

- FS = FS statistics
- x_i = an ordered sample value in a set of n observations sorted in ascending order
- y = calendar year (for years 1991 to 2020 in this study)
- m = calendar month
- N = The resampling rate of the CDF. In our analysis, it is set to 1000 per month.
- $\mathrm{CDF}_m(x_i)$ = long-term CDF for the month m
- $\mathrm{CDF}_{y,m}(x_i)$ = short-term (for the year y) CDF of the daily variable x for the month m

After applying this procedure for each month, Supplementary Material Table S.1 presents the selected typical and extreme representative months for synthetic weather years TMY, ELY, and EHY. Once the representative months are identified, they are aggregated to construct the corresponding representative weather years. The generated TMY, ELY, and EHY are presented in the Supplementary Material Figure S.1.

3.1.3. Extreme weather events method

In identifying the representative historical extreme weather year in Section 3.1.1, we focus on the intensity and duration of extreme periods during which the residual load exceeded the 95th percentile. However, to better understand and assess extreme weather events and their impacts on energy systems, it is crucial to identify specific extreme weather events instead of simplifying them as periods exceeding the 95th percentile. The definition of such events, however, varies significantly across studies [60] and often focuses on meteorological events like heatwaves or windstorms. For example, from an intensity perspective, Li et al. [43] define extreme events as those surpassing the 95th percentile, while from a duration perspective, Mockert et al. [61] characterizes extreme events as lasting a minimum of two consecutive weeks.

In this study, we analyze extreme weather events from the perspective of residual load, focusing on three duration phases: one day, one week, and two weeks. Our objective is to identify the most extreme one-day, one-week, and two-week events across all historical years. To achieve this, we first identify the most extreme one-day, one-week, and two-week events for each historical year, referred to as yearly extreme events. These events are defined as the periods during which the maximum sum of consecutive residual load values occurs within a specified window for that year. For instance, to determine the most extreme one-week event in 1997, we apply a rolling window of one week (168 h) to calculate the consecutive residual load sums throughout the year. Fig. 3 illustrates the consecutive residual load sums for 1997 using this window size. From this figure, we can observe that the maximum residual load sum for a one-week window occurs between hours 97 and 264. This period is identified as the most extreme one-week event for 1997.

After determining the yearly extreme events, we compare them across all 30 historical years to identify the most extreme event overall, defined as the period with the highest residual load sum. Table 2 summarizes the most extreme one-day, one-week, and two-week events across all historical years. These identified extreme events are then used to replace the corresponding periods in the TMY and EHY years generated using the FS statistic method[4]:

- TMY_1D: TMY with the extreme one-day event
- TMY_1W: TMY with the extreme one-week event
- TMY_2W: TMY with the extreme two-week event
- EHY_1D: EHY with the extreme one-day event
- EHY_2W: EHY with the extreme two-week event

[4] No extreme one-week event is replaced in EHY because the most extreme one-week event occurs in January 1997, which is already represented in January of EHY.

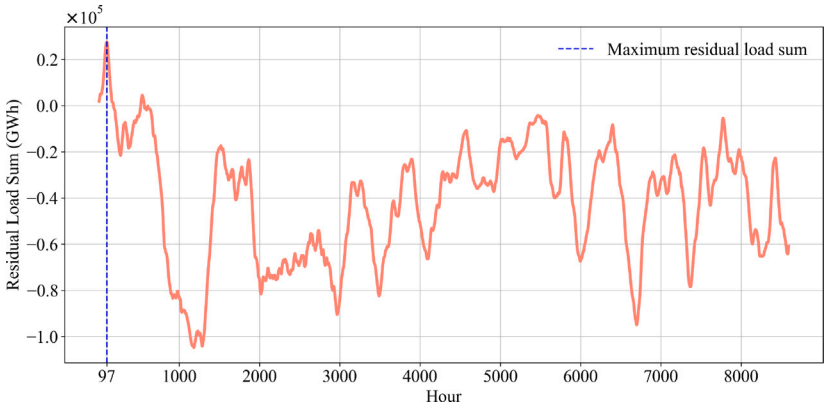

Fig. 3. Consecutive residual load sums for 1997, calculated using a one-week rolling window. The most extreme event begins at hour 97, marking the period with the highest cumulative residual load within this week.

Table 2
The identified most extreme weather events among all historical years.

Events type	Occurred year	Starting hour	Ending hour
One-day event	2017	8463	8486
One-week event	1997	97	264
Two-week event	2002	87	422

Table 3
The capacity values (GW) for renewable energy in the Exogenous-RE scenario, derived from the FlexMex Scenario 4D.

Country	Solar PV	Wind onshore	Wind offshore
Austria	48.8	43.6	0
Belgium	184.1	12.7	11.2
Switzerland	86.2	28.3	0
Czech Republic	38.3	54.0	0
Germany	419.8	233.8	143.9
Denmark	17.7	26.1	1.2
France	279.8	439.9	0
Italy	247.4	247.2	0
Luxembourg	12.4	1.4	0
Netherlands	98.2	21.3	51.2
Poland	77.2	107.0	0

The differences by comparing TMY with TMY_1D, TMY_1W, and TMY_2W, as well as EHY with EHY_1D and EHY_2W are showcased in the Supplementary material Figure S.2.

3.2. Energy system configurations

In this section, we present a detailed overview of the model scope for two renewable capacity expansion scenarios. Additionally, we describe the methodology used to evaluate system robustness.

3.2.1. System configuration scenarios

In the Exogenous-RE scenario, we analyze the energy system model by fixing the capacities for solar PV, onshore wind, and offshore wind based on the values specified in the FlexMex Scenario 4D.[5] By fixing renewable capacities, this scenario aligns with predefined political objectives, such as National Development Plans. Table 3 presents the derived capacity values for solar PV, onshore wind, and offshore wind across the countries in our study. The model scope for Exogenous-RE scenario is illustrated in Fig. 4(a).

In contrast, the Endogenous-RE scenario allows for the endogenous determination of solar PV, onshore wind, and offshore wind capacities. In this scenario, the system optimizes the capacities of renewable energy sources, storage, and flexibility options to minimize overall system costs. This scenario enables the model to explore the most cost-effective combination of renewable and conventional generation, storage, and flexibility solutions to meet system needs, as shown in Fig. 4(b). Meanwhile, we also assign the lower bound values to renewable capacities derived from the International Renewable Energy Agency (IRENA) Renewable Capacity Statistics 2023 [62] to ensure a minimum level of renewable energy generation is maintained. A key challenge in the Endogenous-RE scenario, in contrast to the Exogenous-RE scenario, is that renewable capacities are not predetermined. Since renewable generation is dependent on the installed capacity, the renewable generation time series cannot be determined until the optimization process of the energy system model is finished. Consequently, the residual load can only be calculated after the optimization process is completed. However, it is important to note that the generation of synthetic weather years is still based on residual load values derived from exogenous capacity factors in the Exogenous-RE scenario. As a result, the same synthetic weather years are used for both the Endogenous-RE and Exogenous-RE scenarios.

3.2.2. System robustness evaluation framework

In this section, we describe the process for assessing whether a system configuration can accommodate the conditions of a specific historical year. This process is carried out in two steps using the ESOM REMix.

To evaluate whether the system configuration of year A can accommodate the weather conditions of year B, we first input the weather year dependent time series of year A, including demand, solar PV, wind onshore and offshore profiles, into either the Exogenous-RE or Endogenous-RE scenario, as outlined in Section 3.2.1. This allows us to determine the required capacities for various energy generation, storage, and transmission technologies for year A.

In the second step, we fix the capacities of all technologies, including generation, storage, and transmission lines, based on the values derived from year A. We then input the weather year dependent time series of year B to assess whether the system can accommodate the energy demand under the conditions of year B. To avoid infeasibilities, we introduce slack variables into the model. The slack costs for commodities such as electricity, heat, and hydrogen are set considerably high, ensuring that the optimizer only uses slack when there is no other way to supply demand. If slack appears in the resulting optimal system operation, it indicates that the system configuration optimized for year A is insufficient for year B and vice versa. This is also reflected in a significant increase in system costs due to high slack costs. The model scope for this framework is illustrated in Fig. 5.

[5] FlexMex Scenario 4D assumes endogenous flexibility capacities and targets a 160% VRE penetration, as described in [56].

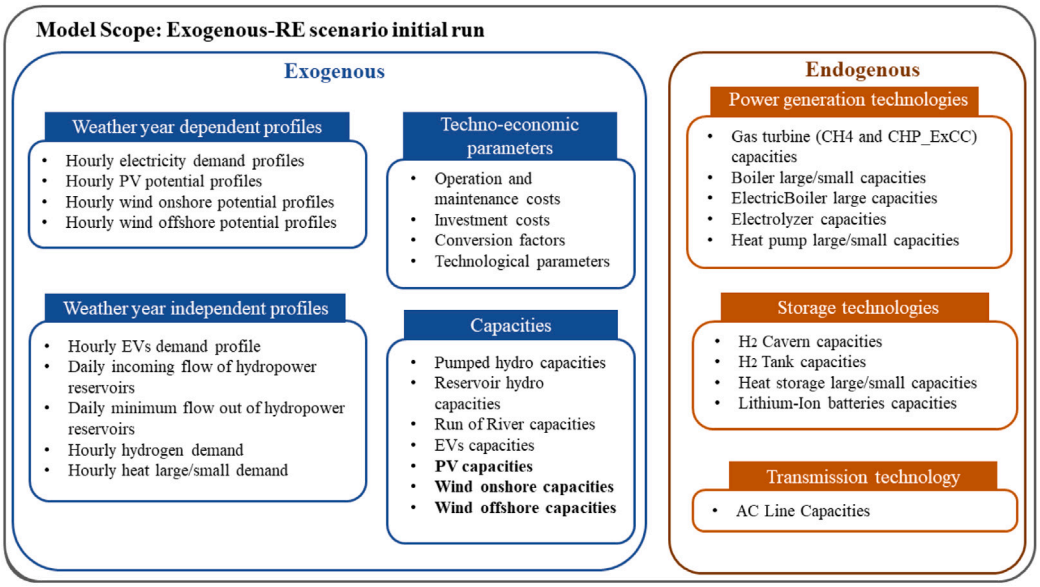

(a) Exogenous-RE scenarios

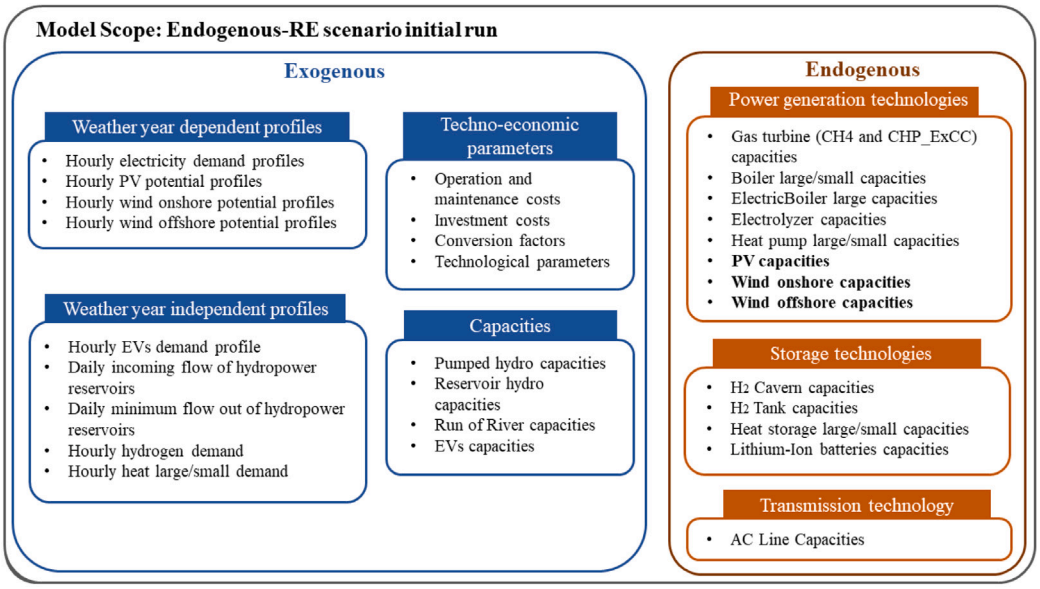

(b) Endogenous-RE scenarios

Fig. 4. The model scope of Exogenous-RE and Endogenous-RE expansion scenarios.

4. Results

To compare the influence of different weather years on the energy system, we assess various indicators, including system costs, annual capacity values, electricity generation, and capacity factors (CF) for different technologies.

4.1. Exogenous-RE expansion scenario

In the initial run of the Exogenous-RE scenario, we input the renewable energy generation and demand time series from both historical and synthetic weather years into the ESOM REMix. Fig. 6 illustrates the system costs across various weather years. From the figure, it is evident that 1997 exhibits the highest system costs among the 30 historical years. In terms of synthetic weather years, EHY, EHY_1D, and EHY_2W result in even higher system costs than 1997, with EHY_1D having the highest system costs. This finding aligns with our earlier residual load analysis in Section 3.1.1, which identified 1997 as the most extreme year. The higher system costs observed for EHY, EHY_1D, and EHY_2W further confirm that the extreme high synthetic weather years, generated using the FS statistic method and the extreme weather events method, also present significant challenges for the energy system.

The capacity values for various power generation technologies are presented in Fig. 7(a). From this figure, we can see the capacities for both PV and wind onshore are the largest among all technologies. In this scenario, since the renewable capacities are fixed, only the gas turbine GH4-GT and CHP-ExCCGT capacities vary across the weather years. Among all historical and synthetic weather years, the highest CH4-GT capacity occurs in 2015, at 273.12 GW, which is nearly 60 GW higher than the second-highest capacity in 2011 (214.80 GW). The lowest CH4-GT capacity is observed in EHY_2W, with only 0.71 GW. However, EHY_2W has the highest CHP-ExCCGT capacity, at 196.82 GW. While other significantly high CHP-ExCCGT years occur in EHY_1D (189.76 GW) and EHY (184.19 GW), years such as ELY and 1999 are among the lowest for CHP-ExCCGT capacity, with values below 1 GW.

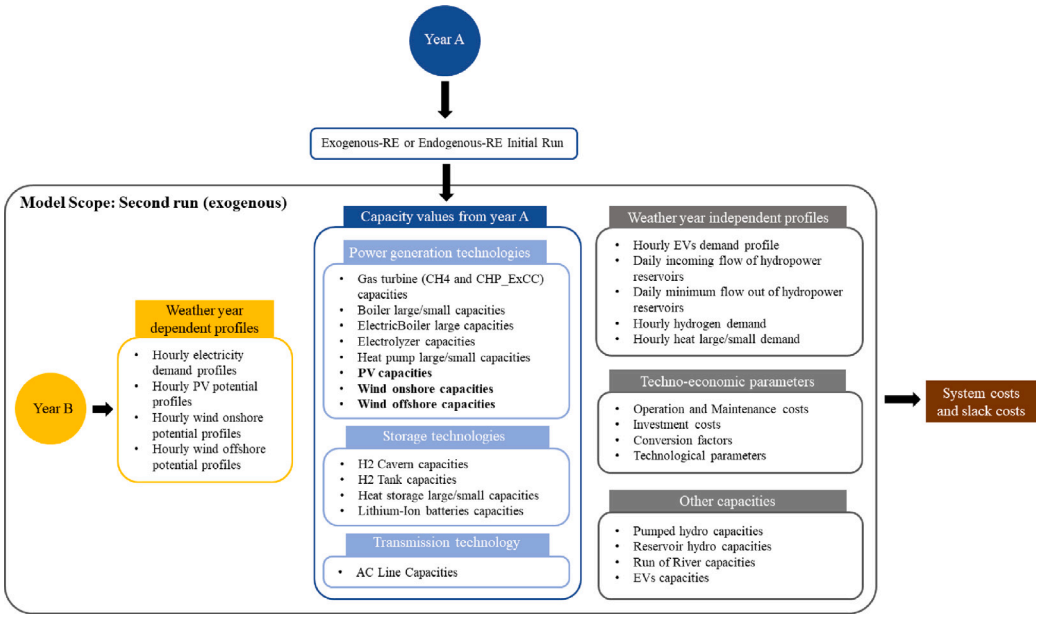

Fig. 5. The model scope for the framework to evaluate the system robustness. This framework is used to determine whether the system configuration of year A can accommodate the weather conditions of year B.

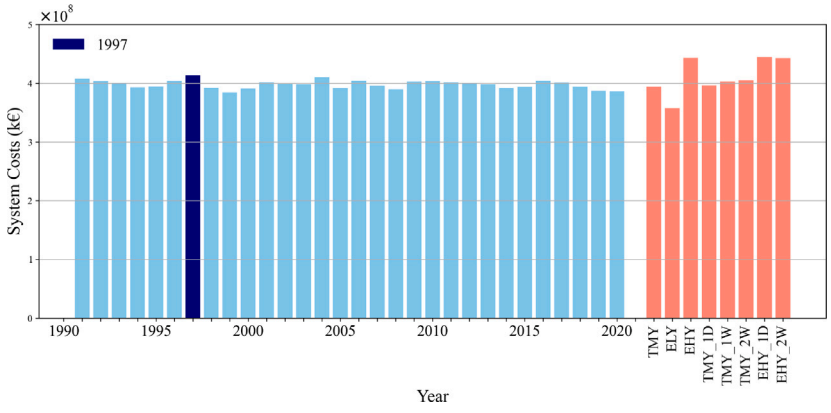

Fig. 6. System costs for various weather years in the Exogenous-RE scenario.

The variation in CH4-GT and CHP-ExCCGT capacities suggests that, although both are dispatchable generation technologies, some years rely more heavily on one technology. To provide a clearer understanding of the dispatchable generation capacities and improve visualization, we aggregate the CH4-GT and CHP-ExCCGT capacity values, as shown in Fig. 7(b). From this figure, it is evident that the highest aggregated gas turbine capacity occurs in 2015, at 280.37 GW, which is about 40 GW higher than the second-highest capacity in TMY_1W (240.44 GW) and the third-highest in 1992 (239.91 GW).

Meanwhile, Figure S.3 in the Supplementary Material illustrates the electricity generation for each weather year. The figure shows that the majority of electricity generation across all weather years comes from PV and onshore wind, with PV generation remaining relatively consistent throughout the years. In addition to these sources, offshore wind and hydropower also contribute a significant share. In contrast, gas turbines CH4-GT and CHP-ExCCGT play a relatively smaller role in the overall electricity generation.

In addition, Fig. 8 presents the corresponding Capacity Factor (CF) for different technologies. Among all technologies, CH4-GT exhibits a relatively low CF, particularly when compared to offshore wind and reservoir hydropower. The highest CF for CH4-GT occurs in the year EHY_2W at 0.078, which corresponds to approximately 483.7 GWh of electricity generation. A similar trend is observed for CHP-ExCCGT, where EHY_2W has the second-highest CF (0.222), slightly lower than the year EHY (0.222), generating approximately 382.3 TWh of electricity. However, in the year EHY_2W, both onshore and offshore wind exhibit some of the lowest CF values, with 0.170 for onshore wind and 0.309 for offshore wind, generating approximately 1812.1 TWh and 561.5 TWh of electricity, respectively. A similar pattern, with relatively high CF for gas turbines and lower CF for wind, is also observed in the years EHY and EHY_1D. This suggests that, under the weather conditions represented by these years, the system relies more heavily on gas turbines to meet demand due to the lower availability of wind energy.

In contrast, for ELY, the CF of gas turbine is the lowest among all years, with 0.044 for CH4-GT and 0.120 for CHP-ExCCGT, generating approximately 66.3 TWh and only 0.6 GWh of electricity, respectively. Meanwhile, the CF for onshore wind (0.292) and offshore wind (0.493) are the highest, generating approximately 3112.3 TWh and 895.1 TWh of electricity, respectively. This indicates that during the weather conditions represented by ELY, the system benefits from high wind generation, reducing the need for gas turbines, implying that ELY represents a year of favorable weather conditions for renewable generation. Meanwhile, it is worth noting that although the capacities

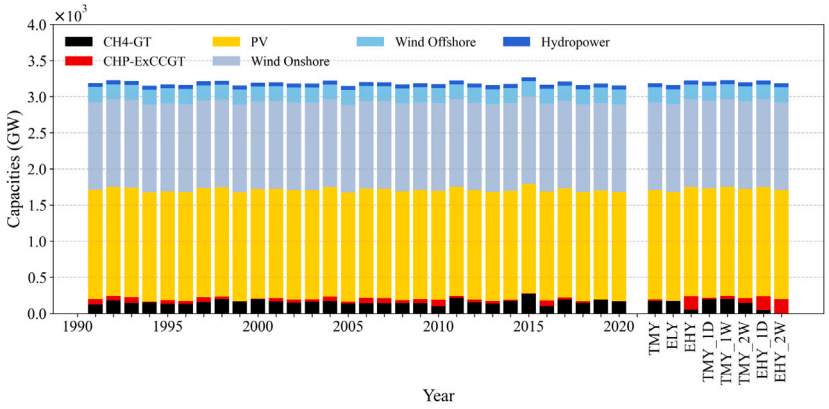

(a) Capacity values for various technologies. For clarity, the capacities of reservoir hydropower and run-of-river hydropower are combined into a single hydropower capacity, as they are relatively low compared to other technologies.

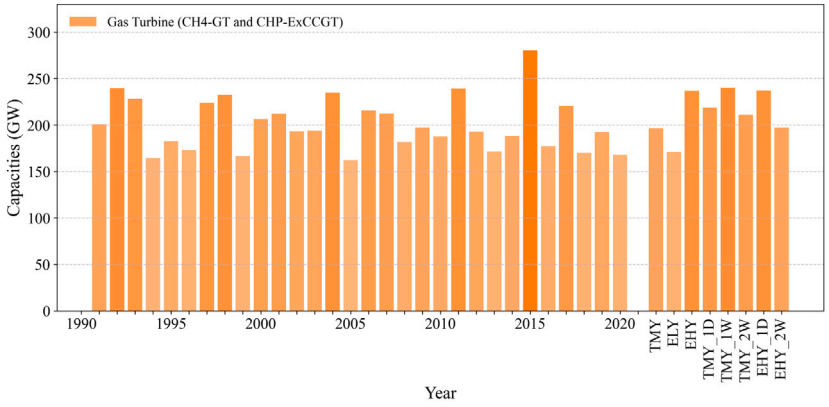

(b) Aggregated capacities of gas turbines CH4-GT and CHP-ExCCGT.

Fig. 7. Capacity values across different weather years in the Exogenous-RE scenario.

of CH4-GT and overall gas turbines are observed to be the highest in 2015, the CF for CH4-GT in 2015 (0.045) is the second lowest among all years, only slightly higher than the lowest CF observed in ELY (0.044), generating approximately 108 TWh of electricity.

To evaluate system robustness, we perform the second model run as described in Section 3.2.2. The robustness of each weather year is presented in the heatmap in Fig. 9. This figure reveals that 2015 is the most robust weather year, as its system configuration can accommodate not only all historical years but also all synthetic weather years. However, none of the other historical or synthetic weather years can accommodate 2015. 1997 ranks as the second most robust year, capable of accommodating 35 out of 38 years, including 27 historical years and all synthetic weather years. Following closely are TMY_1W, 2011, and EHY, accommodating 34, 34, and 33 years, respectively. This outcome is somewhat unexpected, as the extreme years identified and synthesized in Section 3.1 (1997, ELY, EHY_1D, and EHY_2W) fail to accommodate certain historical years. For example, although EHY_2W exhibits the second-highest system costs and the highest CF for gas turbines, it can only accommodate 12 other years. A detailed discussion of this discrepancy is provided in Section 5. Additionally, ELY fails to accommodate any other year, while 2005 and 2008 can only accommodate ELY, making them the least robust years. This observation is consistent with our findings in the previous section.

4.2. Endogenous-RE expansion scenario

In the Endogenous-RE scenario, the system costs for various weather years are presented in Fig. 10. Compared to the Exogenous-RE scenario, the system costs of all weather years are lower in the Endogenous-RE scenario due to the ability to fully optimize the renewable energy capacities and, therefore, adapt to demand in a more cost-efficient way. However, we can reach the same conclusion as the figure reveals that 1997 continues to have the highest system costs among the 30 historical years. Similarly, synthetic weather years EHY, EHY_1D, and EHY_2W also have higher system costs compared to 1997, with EHY_1D being the year with the highest system costs.

The capacity values for various technologies are presented in Fig. 11(a). Similar to the Exogenous-RE scenario, in the Endogenous-RE scenario, PV and onshore wind continue to have the largest capacities compared to other technologies. However, it is worth noting that offshore wind capacity for all weather years is just 16.43 GW, which is the lower bound set for this scenario. This limited expansion is mainly due to the high costs of offshore wind turbines compared to other renewable energy technologies. Meanwhile, we can also observe that the onshore wind capacities remain relatively consistent across the weather years, which is not the case for PV capacities. Compared to other years, PV capacities are significantly higher in the years EHY_2W (2122.5 GW), EHY_1D (2101.3 GW), and EHY (2085.2 GW). This is likely due to the limited wind availability in these years, and the system compensates for these extreme conditions by expanding PV as a cost-effective solution to mitigate the impact of persistent high residual load periods. Regarding gas turbines, the largest CH4-GT capacity is observed in 2000, with approximately 202.9 GW, followed by 2015 at 189.8 GW, and TMY_1W with 142.4 GW. For CHP-ExCCGT, the largest capacity is found in EHY_2W (157.7 GW), followed by EHY_1D (148.0 GW) and EHY (142.5 GW).

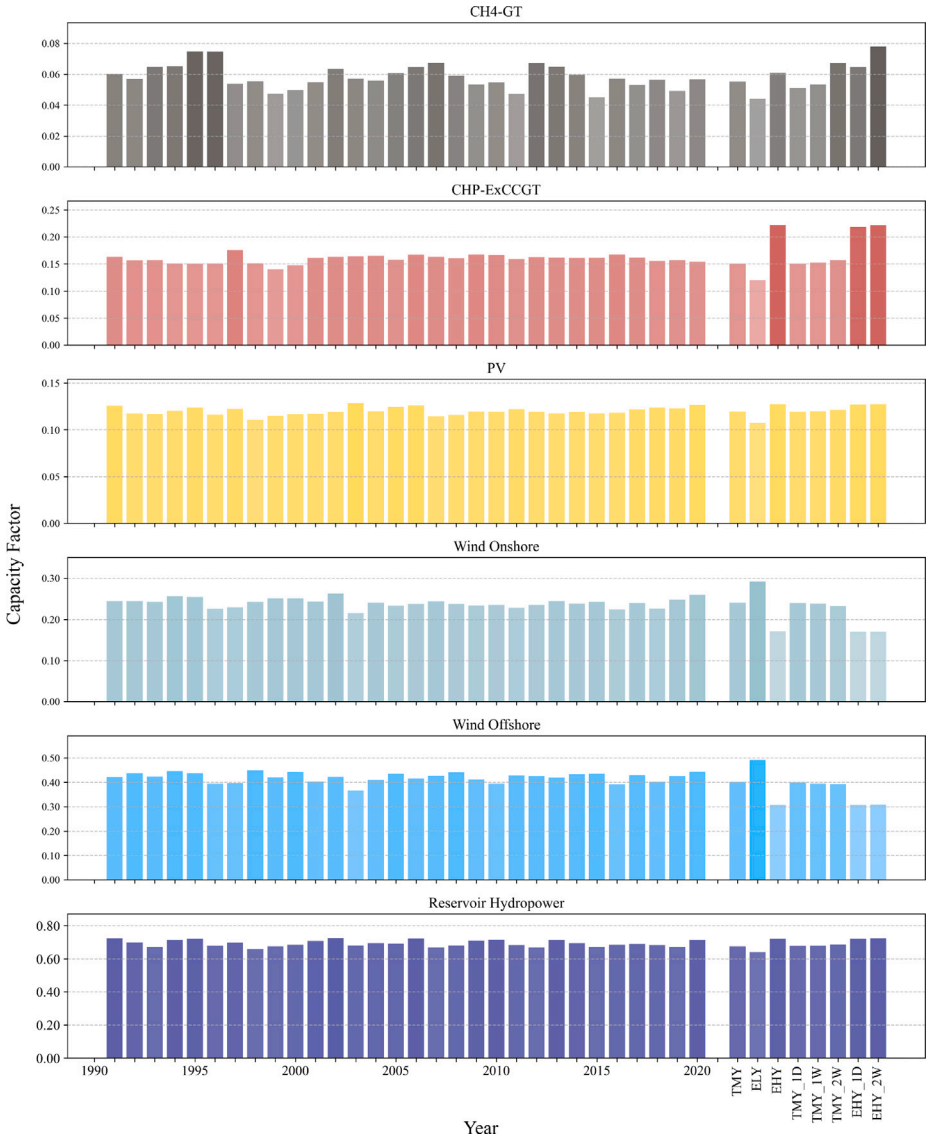

Fig. 8. Capacity factors for various technologies across different weather years in the Exogenous-RE scenario. The capacity factor for Run-of-river hydro is constant at 1 across all weather years and is therefore not displayed in the figure.

Similar to the Exogenous-RE scenario, the aggregated gas turbine capacities are shown in Fig. 11(b). The lowest gas turbine capacity is observed in ELY, with only 113.79 GW, while the highest capacity occurs in 2004, at 263.6 GW, followed by 2015 (249.7 GW) and 1992 (229.6 GW). These values are lower than those in the Exogenous-RE scenario, where 2015 exhibits the highest gas turbine capacity at 280.37 GW.

Meanwhile, Figure S.4 in the Supplementary Material illustrates the electricity generation across different weather years. From this figure, it is clear that the majority of electricity generation comes from PV and onshore wind. The increased electricity generation from PV in the years EHY, EHY_1D, and EHY_2W further indicates the system's reliance on PV expansion to compensate for high residual load conditions.

Fig. 12 presents the CF for various technologies across different weather years. In this scenario, TMY_2W exhibits the highest CF for CH4-GT at 0.075, generating around 49.5 TWh of electricity. Other years with high CH4-GT CF include 2006 (0.074), 1995 (0.073), and 1996 (0.073), while the lowest CF is observed in 2004 at 0.043, generating 53.6 TWh of electricity. For CHP-ExCCGT, similar to the Exogenous-RE scenario, the significantly high CF is observed in the years EHY (0.218), EHY_1D (0.217), and EHY_2W (0.215), generating 272.5 TWh, 281.7 TWh, and 296.6 TWh of electricity, respectively. The lowest CF is observed in ELY (0.134), generating only 1.4 GWh of electricity.

As with the Exogenous-RE scenario, the CF for PV remains relatively consistent across all weather years. In contrast, onshore and offshore wind show low CF in the years EHY (0.191 and 0.315 for onshore and offshore wind, respectively), EHY_1D (0.191 and 0.315), and EHY_2W (0.191 and 0.317), generating 1887.7 TWh, 1857.1 TWh, and 1818.4 TWh from onshore wind, and 45.4 TWh, 45.3 TWh, and 45.6 TWh from offshore wind, respectively. In contrast, ELY exhibits the highest CF for wind energy, with 0.418 for onshore wind and 0.539 for offshore wind, generating 3745.0 TWh and 77.5 TWh of electricity, respectively, further indicating that ELY represents a year with favorable weather conditions for wind generation. Furthermore, similar to the case of 2015 in the Exogenous-RE scenario, while 2004 has the highest overall gas turbine capacity, its CH4-GT CF (0.043) is the lowest among all years, and the CHP-ExCCGT CF (0.183) ranks in the middle, generating 250.4 TWh electricity in total.

For the second model run, the results are presented in the heatmap in Fig. 13. This figure reveals that 2004 is the most robust year, capable

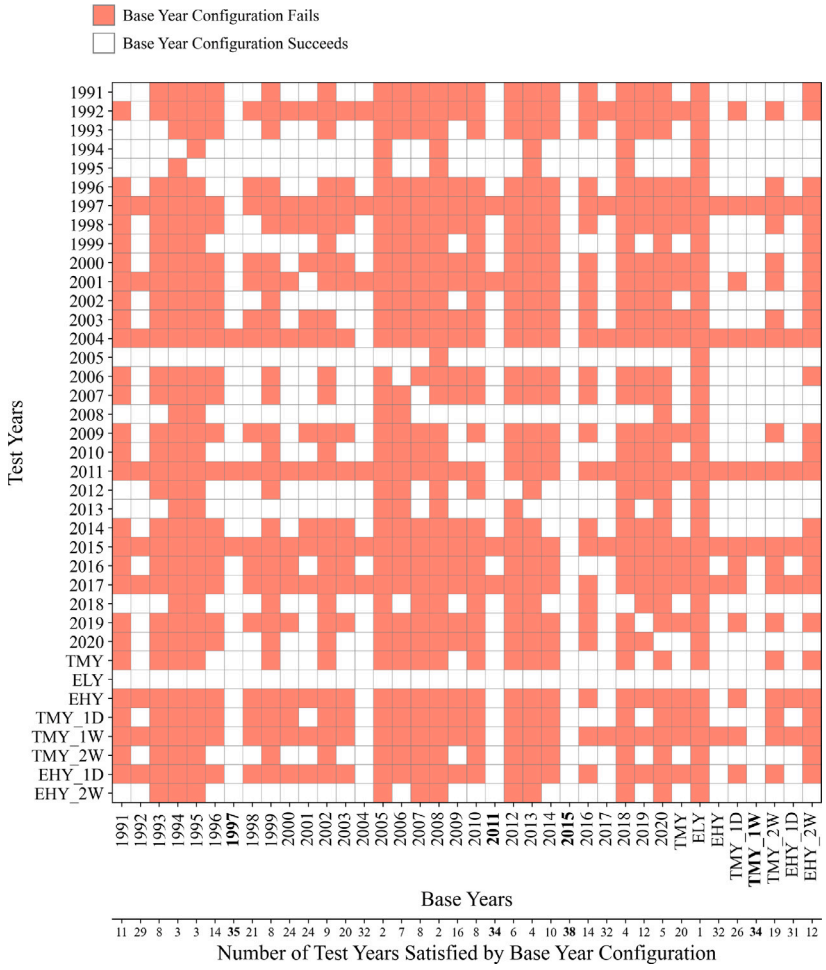

Fig. 9. Heatmap showing the ability of energy system configurations based on different base years in the Exogenous-RE scenario to accommodate various test years. The x-axis at the bottom quantifies the total number of test years satisfied by each base year configuration.

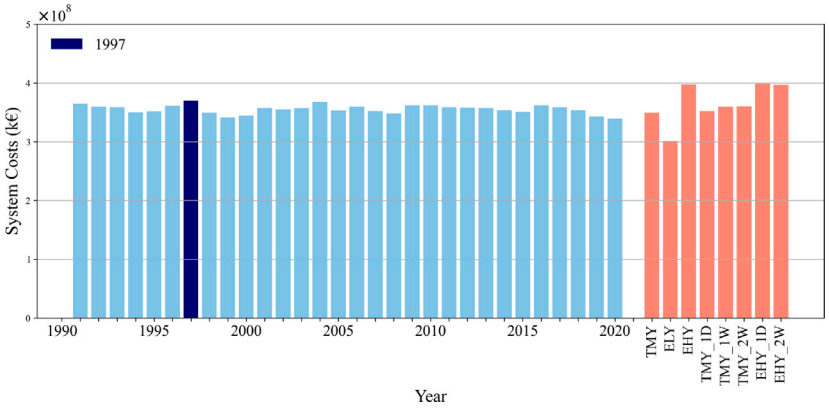

Fig. 10. System costs for various weather years in the Endogenous-RE scenario.

of accommodating all historical and synthetic weather years. 1992 and 2015 emerge as the second most robust years, each accommodating 34 weather years. Close behind are 1997, 2001, and TMY_1W, each capable of accommodating 32 years. Additionally, similar to the Exogenous-RE scenario, ELY is the least robust year, as it fails to accommodate any other years.

5. Discussion and limitations

5.1. Impact of gas turbine usage on system costs

From the previous analysis, we can identify that the years 1997, EHY, EHY_1D, and EHY_2W exhibit higher system costs compared to

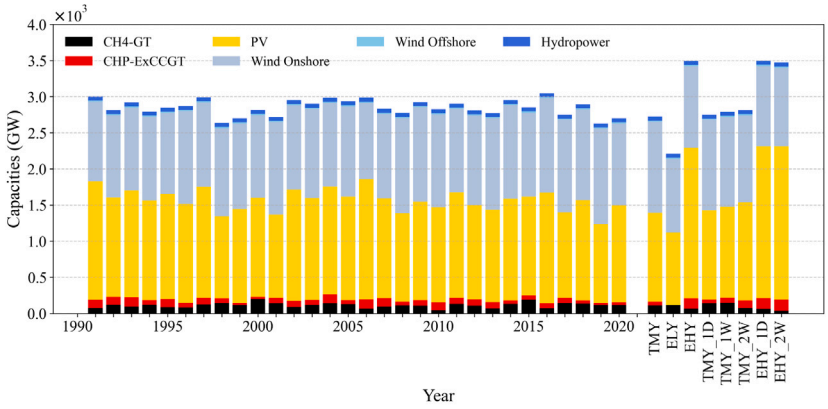

(a) Capacity values for various technologies. For clarity, the capacities of reservoir hydropower and run-of-river hydropower are combined into a single hydropower capacity, as they are relatively low compared to other technologies.

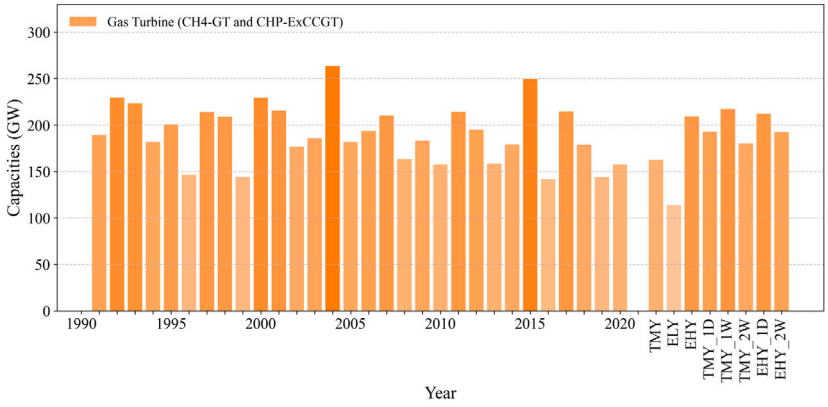

(b) Aggregated capacities of gas turbines CH4-GT and CHP-ExCCGT.

Fig. 11. Capacity values across different weather years in the Endogenous-RE scenario.

other years in both scenarios. Meanwhile, they also show a significantly better ability to accommodate other years. As shown in the heatmaps in Figs. 9 and 13, in the Exogenous-RE scenario, the traditional TMY method can accommodate 20 other years, whereas 1997 can accommodate 35 years. The proposed synthetic weather year methods also perform well, with EHY accommodating 32 years, and EHY_1D accommodating 31 years. Similarly, in the Endogenous-RE scenario, the traditional TMY method accommodates only 3 other years, while 1997 accommodates 32 years, and both EHY and EHY_1D accommodate 29 years. These results demonstrate that our identified extreme year and the generated synthetic weather years are significantly more robust than the traditional TMY.

In addition, we can also observe a strong correlation between system costs and the usage of gas turbines. As the usage of gas turbines increases, reflected by higher gas turbine CF, the system relies more on gas turbine operation, leading to higher fuel consumption and carbon costs. In contrast, years with low usage of gas turbines, characterized by lower gas turbine CF, such as ELY in both scenarios, tend to have greater contributions from abundant renewable energy generation, thus having the lowest system costs. The scatter plots in Figure S.5 of the Supplementary material confirm this relationship, showing a high positive correlation between the overall gas turbine CF of both CH4-GT and CHP-ExCCGT and system costs, with Correlation Coefficients (CC) of 0.89 in the Exogenous-RE scenario and 0.83 in the Endogenous-RE scenario. This finding is consistent with previous studies. For example, Bagga et al. [63] estimate a substantial increase in total system costs under low and medium renewable energy scenarios, primarily driven by the higher fuel costs of dispatchable generation technologies.

5.2. Impact of gas turbine capacities on system robustness

However, higher system costs do not necessarily indicate a more robust system. As shown in the previous sections, 2015 in the Exogenous-RE scenario and 2004 in the Endogenous-RE scenario are the most robust weather years. A common factor between these years is that their aggregated gas turbine capacities are the highest among all historical years. This relationship is further illustrated in the scatter plot in Fig. 14, which depicts the correlation between the aggregated gas turbine capacity and the number of years satisfied. In the Exogenous-RE scenario, the CC is 0.83, while in the Endogenous-RE scenario, it is 0.82. These high correlation coefficients also indicate a strong positive correlation between gas turbine capacity and a year's ability to accommodate other years, suggesting that higher gas turbine capacities increase the likelihood of accommodating other years. The importance of dispatchable generation in mitigating the variability and intermittency of renewable energy sources, and thereby enhancing the flexibility and robustness of the energy system, has been widely examined in recent literature [64–66]. For example, Wang et al. [67] emphasized the critical role of gas turbines with robust starting, fast ramp rates, and high thermal efficiency, which make them well-suited for managing peak loads and supporting overall system stability.

In addition to having the highest gas turbine capacities, 2015 and 2004 share another characteristic: the CF for gas turbines, especially the CH4-GT, is relatively low compared to other years. This indicates that, despite their substantial gas turbine capacities, these turbines are less frequently used throughout the year. Similar observations are reported in previous studies [68,69], which demonstrate that although

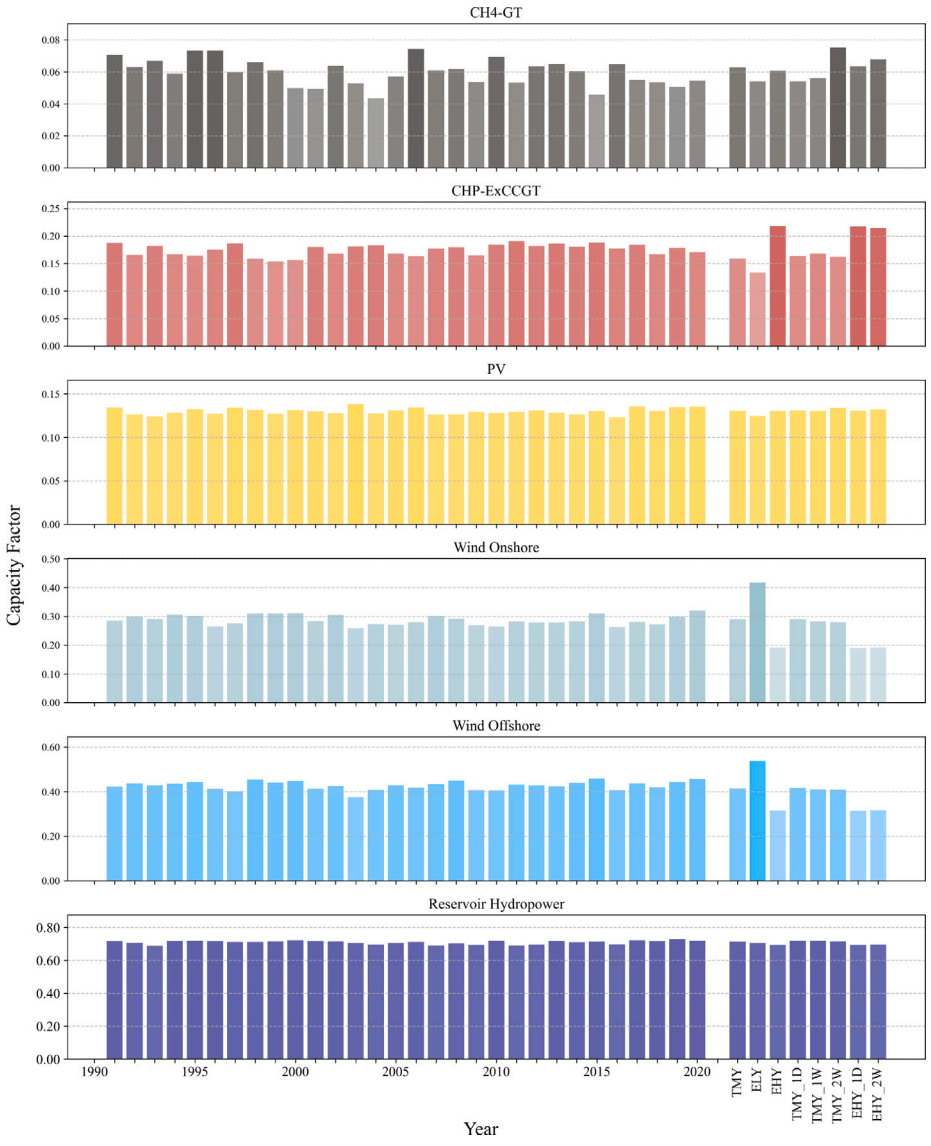

Fig. 12. Capacity factors for various technologies across different weather years in the Endogenous-RE scenario. The capacity factor for Run-of-river hydro is constant at 1 across all weather years and is therefore not displayed in the figure.

gas turbines may exhibit low annual usage, they play a critical role in ensuring power system reliability. These findings indicate that there may be severe extreme periods within the year that require such a high gas turbine capacity to satisfy the demand. In other words, their operation is likely required for specific short-term periods of high demand or low renewable generation, rather than sustained, prolonged usage.

Meanwhile, it is evident that more robust years, such as 2015 and 2004 in their respective scenarios, tend to rely more on CH4-GT, whereas years with high system costs and prolonged periods of high residual load, such as EHY, EHY_1D, and EHY_2W, predominantly use CHP-ExCCGT. This is likely due to the characteristics of these gas turbines. In our model, CHP-ExCCGT has higher investment costs compared to CH4-GT. For years with short-term periods of high residual load, CH4-GT is the more favorable option due to its lower costs [70]. However, when a year experiences prolonged periods of high residual load, the system favors CHP-ExCCGT, as it can provide both electricity and heat, making it a more cost-effective choice in the long run.

5.3. Impact of short-term events on gas turbine capacities

To investigate whether 2015 and 2004 exhibit short-term extreme events that are the most severe among historical years, we analyze the periods where the energy system configuration, optimized for years like 1997, fails to accommodate 2015 and 2004 in their respective scenarios. Specifically, we examine periods with high slack values in the optimization results.

Our results reveal that, in the Exogenous-RE scenario, the system configuration of 1997 is unable to accommodate 2015 during a critical 16-h period (i.e., hours 1002 to 1017). To assess the extremity of this period, we roll a 16-h window across the residual load time series in 2015 and identify that the most extreme 16-h period indeed occurs between hours 1002 and 1017, as shown in Figure S.6a in the Supplementary Material. This period not only represents the most critical window in 2015 but also the most extreme across all historical years, as illustrated in Figure S.7a in the Supplementary Material, which compares the cumulative residual load for the 16-h window across all years. Similarly, in the Endogenous-RE scenario, the system

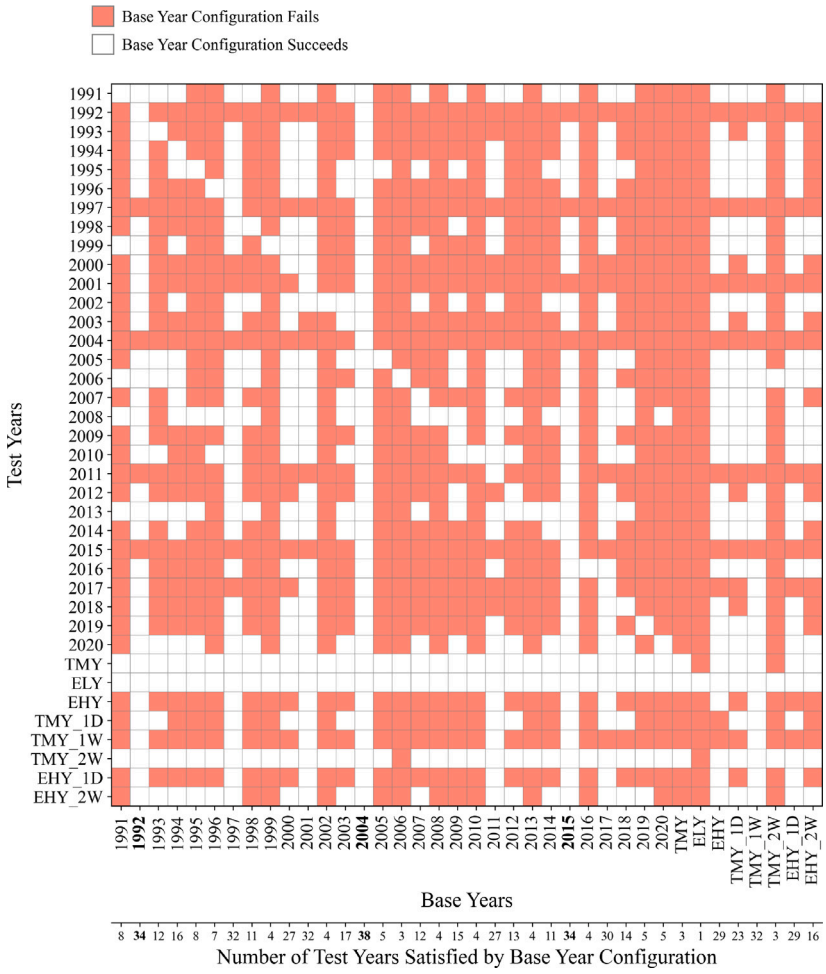

Fig. 13. Heatmap showing the ability of energy system configurations based on different base years in the Endogenous-RE scenario to accommodate various test years. The x-axis at the bottom quantifies the total number of test years satisfied by each base year configuration.

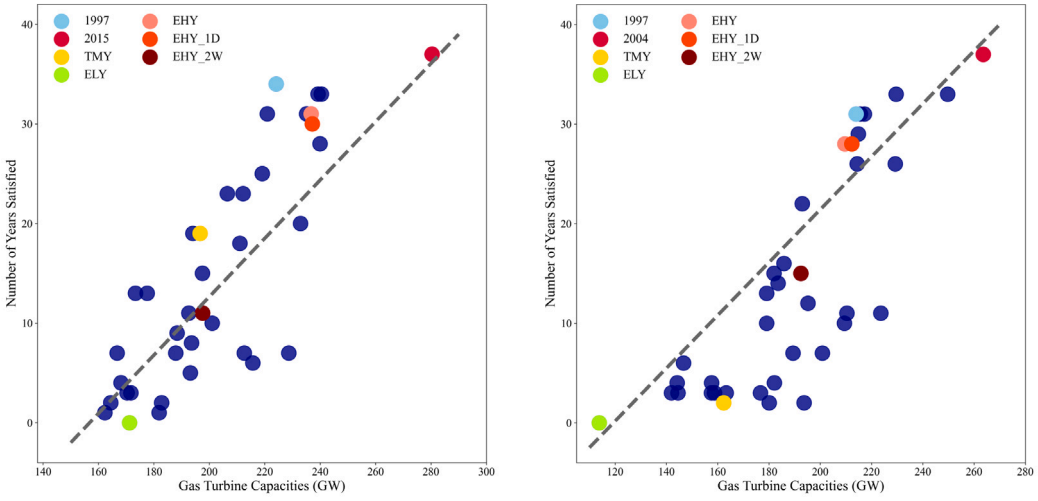

(a) Exogenous-RE scenario (CC = 0.83) (b) Endogenous-RE scenario (CC = 0.82)

Fig. 14. Scatter plots showing the relationship between aggregated gas turbine capacities and the number of years satisfied. Years with low gas turbine capacity, such as ELY, fail to accommodate any other years, while years with high gas turbine capacity, such as 2015 in the Exogenous-RE scenario and 2004 in the Endogenous-RE scenario, can accommodate all other weather years.

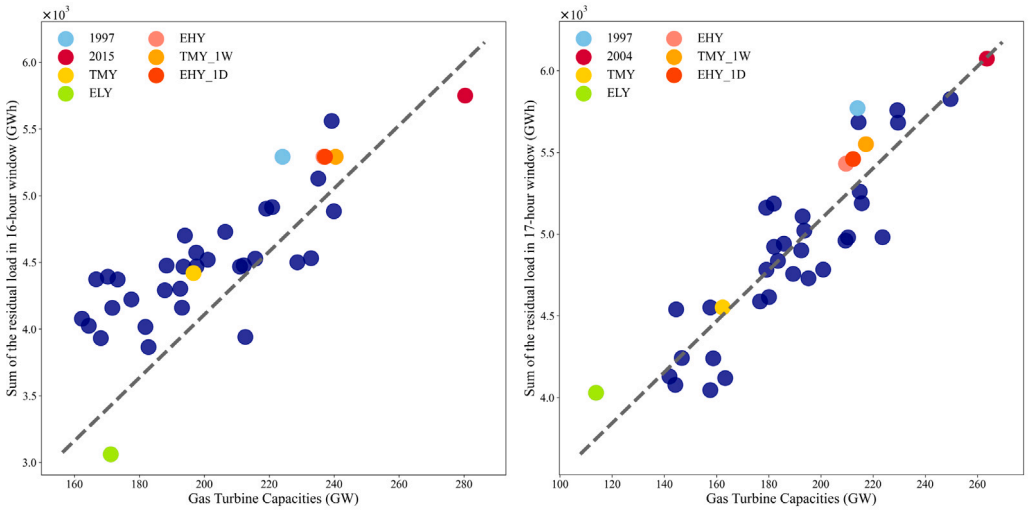

(a) Exogenous-RE scenario (CC=0.82) (b) Endogenous-RE scenario (CC=0.90)

Fig. 15. Scatter plots showing the relationship between the severity of extreme weather events and gas turbine capacity, with a fixed window size. Years with low gas turbine capacity, such as ELY, exhibit low cumulative residual load, while years with high gas turbine capacity, such as 2015 and 2004 in their respective scenarios, show high cumulative residual load.

configuration of 1997 fails to accommodate 2004 due to a 17-h critical period (i.e., hours 8321 to 8337). Our analysis identifies this as the most extreme 17-h event in 2004 and across all historical years, as shown in Figure S.6b and Figure S.7b in the Supplementary Material.

These findings indicate the importance of short-term extreme events. In fact, the intensity of these events is closely correlated with gas turbine capacities, as indicated in Fig. 15. In the Exogenous-RE scenario, the CC is 0.82, and in the Endogenous-RE scenario, it is 0.90. These correlations suggest that the intensity of these short-term extreme events necessitates high gas turbine capacity, thereby contributing to the system's robustness in accommodating a broader range of years.

5.4. Window size selection for short-term events

In our analysis, we identify 16-h and 17-h windows as critical for the Exogenous-RE and Endogenous-RE scenarios, respectively. The intensity of extreme events within these windows strongly correlates with gas turbine capacity and, consequently, influences system robustness. However, to determine whether these are the only influential window sizes or if other durations better represent the extremity of extreme events, we conduct a further analysis.

We begin by examining the CC between extreme event intensity and gas turbine capacity as a function of window size as indicated in Figure S.8 in the Supplementary Material. Our results reveal that the window sizes yielding the highest CC are 17 h in the Exogenous-RE scenario and 18 h in the Endogenous-RE scenario. This suggests that while our initially identified windows are close to optimal, slightly longer windows may better capture the impact of extreme events on system robustness.

Additionally, Fig. 16 ranks the weather years based on the severity of the extreme events across different window sizes. In the Exogenous-RE scenario, 2015 is the most extreme year in terms of short-term extreme events for window sizes between 14 and 18 h, while 1997 stands out for its long-term extreme events, particularly for window sizes between 100 to 200 h and 600 to 1000 h. In the Endogenous-RE scenario, 2004 is the most extreme year for short-term events within the 16 to 20-h window size.

5.5. Insights and limitations

In this study, we propose several methods to identify and generate representative weather years that account for extreme weather conditions across all historical years. These methods are tested across two energy system configuration scenarios using a two-step approach. Our results reveal that traditional methods, such as TMY, fail to induce power supply configurations that can accommodate the majority of weather years, indicating the need for more representative years that capture extreme conditions relevant to energy system modeling.

Our analysis reveals a strong correlation between gas turbine capacity and system robustness, indicating that short-term extreme events are more critical in terms of system robustness to weather. While long-term extreme events, such as those observed in 1997, EHY, EHY_1D, and EHY_2W, increase gas turbine usage throughout the year and lead to higher system costs, these higher costs do not necessarily guarantee a robust system. In contrast, years such as 2015 and 2004, within their respective scenarios, exhibit greater robustness due to their high gas turbine capacities needed to compensate for short-term extreme events.

For energy system modelers, recognizing and identifying years with significant short-term extreme weather events like 2015 and 2004 is essential for selecting representative or extreme years for modeling. Among the various methods for generating synthetic weather years, including those applied in this study, the specific choice of time horizons, like one day, one week, or two weeks, does not necessarily guarantee a system-robust year for energy system optimization. Instead, our findings suggest that a 17-h or 18-h window is the most suitable duration for detecting critical extreme events in their respective scenarios. This insight can serve as a guideline for modelers to effectively capture critical extreme weather conditions.

However, it is worth noting that while years with extreme long-term events like 1997 and EHY may not accommodate all historical years, they can still accommodate the majority of the years. This is particularly relevant in Endogenous-RE scenarios, where calculations of residual load before running the optimization process are uncertain and thus do not allow for the exact identification of extreme events.

One key limitation of our approach is the lack of spatial resolution in the analysis. Extreme events identified in the overall residual load

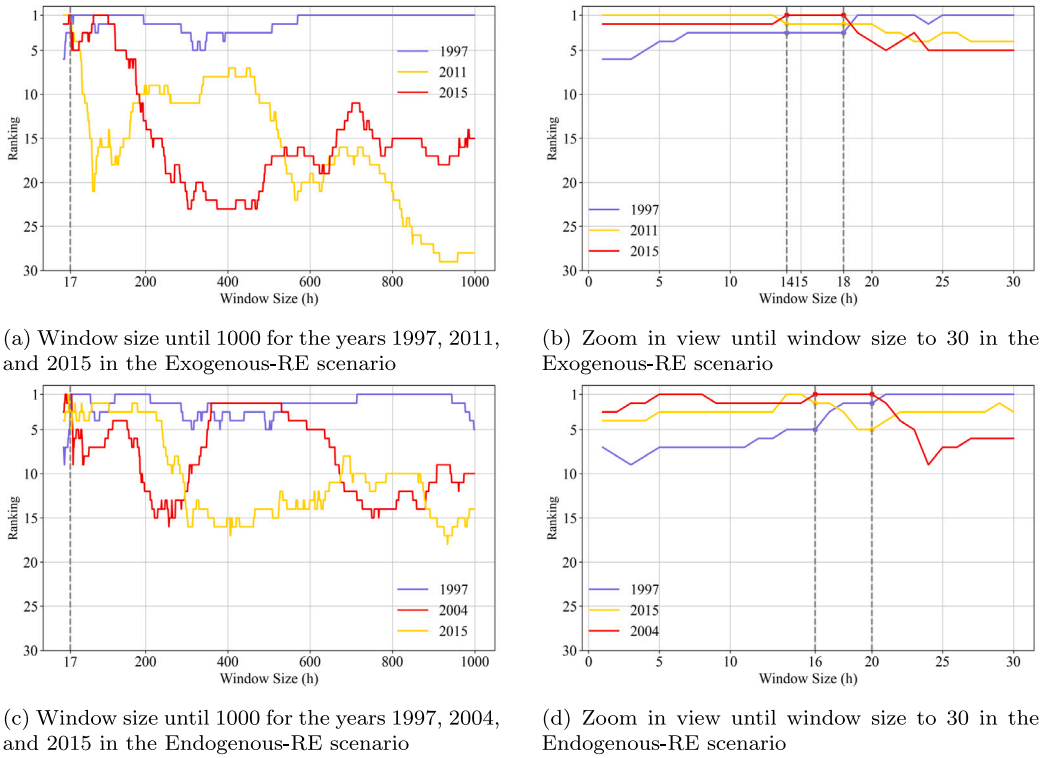

(a) Window size until 1000 for the years 1997, 2011, and 2015 in the Exogenous-RE scenario

(b) Zoom in view until window size to 30 in the Exogenous-RE scenario

(c) Window size until 1000 for the years 1997, 2004, and 2015 in the Endogenous-RE scenario

(d) Zoom in view until window size to 30 in the Endogenous-RE scenario

Fig. 16. Ranking of the selected weather years based on the intensity of extreme events across various window sizes for Exogenous-RE and Endogenous-RE scenarios.

do not necessarily reflect similar patterns in each country within the model. Different countries, and even distinct regions within the same country, may experience diverse weather conditions due to variations in climate zones [71], monsoon [72,73], and temperate marine climates [74]. Additionally, differences in energy system structures [75], energy policies [76,77], and demand patterns [78,79] could further affect the residual load in different ways. Future work should incorporate higher spatial resolution weather data, as demonstrated by studies such as [80,81], and increase the number of nodes representing sub-regions within countries [82,83] to provide a more detailed understanding of how extreme events affect different regions and improve the applicability of the findings.

Another limitation lies in the definition of extreme events, which varies significantly across studies. In our study, we identify two types of extreme events to generate synthetic weather years. The first, introduced in Section 3.1.1, defines extreme conditions as periods where residual load exceeds the 95th percentile of all historical residual loads. The second, described in Section 3.1.3, identifies one-day, one-week, and two-week extreme events based on the periods with the maximum consecutive residual load across all years. However, there is currently no widely recognized framework for defining and quantifying weather conditions in the context of energy systems [60]. Once such a standardized approach is established, future research could align the criteria used in this study with widely recognized definitions, thereby making the generated synthetic weather years more reliable and consistent with established standards.

Additionally, while our synthetic weather years are designed to represent extreme conditions, they may not fully capture the variability of extreme events in reality. These synthetic years could be overly generalized or may fail to capture other critical short-term extreme events that are not presented in our analysis. Furthermore, the deterministic approach used in this study may not reflect long-term variability in climate patterns, potentially leading to less accurate representations of extreme conditions. Future research could explore stochastic methods to provide a more comprehensive investigation of synthetic weather years and better account for the uncertainty and variability in climate data.

Meanwhile, although this study includes two key dispatchable generation technologies, namely CH4-GT and CHP-ExCCGT, it is limited in the scope of dispatchable technologies considered. Other low-carbon dispatchable options, such as biomass-based CHP or storage-integrated thermal power plants, are not included. These technologies could play a critical role in enhancing system robustness, particularly under high-renewable scenarios, by providing seasonal or flexible backup capacity [84–86]. Future research should expand the technology scope to include such options, allowing for a more comprehensive assessment of system robustness and reducing potential bias toward fossil-based solutions.

Our approach also reveals that extreme weather events, particularly short-term events, are key factors of system robustness. However, it is important to note that demand-side management, such as demand shifting, shedding, or time-of-use pricing is not considered within the scope of our model. While short-term extreme weather events play a critical role in determining system robustness, demand-side management could be employed to mitigate the impacts of these extreme periods by reducing peak loads and enhancing system flexibility [87–89]. Once short-term events are mitigated using such techniques, long-term extreme weather events could become more critical for the system's robustness, as they may require sustained capacity adjustments over extended periods. Future work should consider integrating demand-side management measures and exploring their synergies with storage and dispatchable generation to better assess system robustness under both short- and long-duration extreme events.

Meanwhile, sector-coupled energy systems are highly sensitive to inputs and the model scope. The complex interactions between system components can either mitigate or amplify the impact of extreme weather events. For example, while 17-h and 18-h extreme events are critical in our findings, other factors, such as various storage technologies, might play an important role in mitigating the short-term extreme events. However, we find that the storage capacities do not significantly

affect the handling of short-term extreme events, as shown in Figure S.9 and Figure S.10 in the Supplementary Material. This suggests that, within such short time frames and with events encompassing a wide geographical scope, gas turbines are more competitive than storage technologies. Future studies could explore scenarios where storage technologies become more competitive and investigate their role in enhancing the system's robustness. Similarly, incorporating a wider range of dispatchable generation technologies, including geothermal energy, biomass energy, and nuclear power, as applicable, in the assessment can enhance the understanding of system operation and improve flexibility during periods of low wind and solar resource availability.

Besides the storage technologies, renewable energy performance or broader geospatial scope may also significantly influence the system's robustness. These additional factors could lead to different results and conclusions. Future research may also aim to identify a minimum viable model scope that can effectively capture the influence of extreme weather events. This would isolate the impact of short-term extreme events by eliminating the influence of other factors, providing a clearer understanding of their role in system robustness. As model complexity increases, more comprehensive analyses are needed to investigate the interaction between extreme weather events and system components. This simplified model could serve as a foundational tool for identifying critical weather patterns and their impacts without the complexity of full-scale sector coupling. Building on the findings of this study, future research can refine methodologies for designing robust energy systems that are resilient to a wide range of extreme weather conditions.

6. Conclusion

This study indicates the critical role of short-term extreme weather events, with durations of less than a day, in influencing the capacities of dispatchable generation technologies, such as gas turbines, and therefore determining the robustness of energy system designs to different weather conditions. By generating and applying 30 historical and 8 synthetic weather years in two energy system configuration scenarios, Exogenous-RE and Endogenous-RE scenarios, we demonstrate that traditional approaches like Typical Meteorological Year (TMY), as well as contemporary methods for creating synthetic weather years, fail to fully capture the extreme conditions required for designing weather-robust systems. For example, TMY can accommodate only 20 years in the Exogenous-RE scenario and just 3 years in the Endogenous-RE scenario, respectively. Our assessment shows that robust energy systems exhibit the highest gas turbine capacities, with 280.4 GW in the Exogenous-RE scenario and 263.6 GW in the Endogenous-RE scenario. These systems are designed using years with the most extreme short-term events among all historical years, such as 2015 in the Exogenous-RE scenario and 2004 in the Endogenous-RE scenario. This reveals the strong correlation between capacities of dispatchable generation, short-term extreme events, and system robustness. These findings can assist modelers in selecting or synthesizing weather years for energy system optimization or simulations, especially when designing systems that are robust to extreme weather conditions.

CRediT authorship contribution statement

Wenxuan Hu: Writing – original draft, Visualization, Validation, Methodology, Investigation, Formal analysis, Data curation, Conceptualization. **Yvonne Scholz:** Writing – review & editing, Validation, Supervision, Project administration, Methodology, Funding acquisition, Conceptualization. **Madhura Yeligeti:** Writing – review & editing, Methodology, Investigation. **Eugenio Salvador Arellano Ruiz:** Writing – review & editing, Methodology. **Patrick Jochem:** Writing – review & editing, Supervision, Methodology, Funding acquisition.

Declaration of competing interest

The authors declare that they have no known competing financial interests or personal relationships that could have appeared to influence the work reported in this paper.

Acknowledgments

This study builds on the foundation of the VERMEER project (03EI1010A) funded by the Federal Ministry for Economic Affairs and Climate Action (BMWK) of Germany, and received further funding from DESYS, the Energy Program of the German Aerospace Center (DLR) in 2025. Thanks also to Viktor Slednev, our colleague from the Karlsruhe Institute of Technology (KIT), for providing the demand time series data and valuable discussions. Additional thanks to Hans Christian Gils and other members of the REMix development team at the German Aerospace Center (DLR) for their contributions to this work.

Appendix A. Supplementary data

Supplementary material related to this article can be found online at https://doi.org/10.1016/j.solener.2025.113984.

Data availability

All the raw demand and power generation time series, as well as the generated representative weather years time series, are provided in Zenodo at the following URL: https://zenodo.org/records/14983895 or DOI:10.5281/zenodo.14983895.

References

[1] T. Brown, J. Hörsch, D. Schlachtberger, PyPSA: Python for power system analysis, 2017, arXiv preprint arXiv:1707.09913.
[2] S. Sinha, S. Chandel, Review of recent trends in optimization techniques for solar photovoltaic–wind based hybrid energy systems, Renew. Sustain. Energy Rev. 50 (2015) 755–769.
[3] S. Pfenninger, A. Hawkes, J. Keirstead, Energy systems modeling for twenty-first century energy challenges, Renew. Sustain. Energy Rev. 33 (2014) 74–86.
[4] S. Janjai, P. Deeyai, Comparison of methods for generating typical meteorological year using meteorological data from a tropical environment, Appl. Energy 86 (4) (2009) 528–537.
[5] H.Ü. Yilmaz, E. Fouché, T. Dengiz, L. Krauß, D. Keles, W. Fichtner, Reducing energy time series for energy system models via self-organizing maps, IT-Inf. Technol. 61 (2–3) (2019) 125–133.
[6] K. Knight, S. Klein, J. Duffie, A methodology for the synthesis of hourly weather data, Sol. Energy 46 (2) (1991) 109–120.
[7] A.L. Chan, T.-T. Chow, S.K. Fong, J.Z. Lin, Generation of a typical meteorological year for Hong Kong, Energy Convers. Manage. 47 (1) (2006) 87–96.
[8] Y. Wu, J. An, C. Gui, C. Xiao, D. Yan, A global typical meteorological year (TMY) database on ERA5 dataset, in: Building Simulation, Vol. 16, Springer, 2023, pp. 1013–1026.
[9] K.T. Huang, W.S. Ou, Using modified sandia method in developing typical solar radiation year for photovoltaic electricity generation projection, Appl. Mech. Mater. 71 (2011) 4374–4381.
[10] B. Qian, R. De Jong, J. Yang, H. Wang, S. Gameda, Comparing simulated crop yields with observed and synthetic weather data, Agricult. Forest. Meterol. 151 (12) (2011) 1781–1791.
[11] L. Kuchar, Using WGENK to generate synthetic daily weather data for modelling of agricultural processes, Math. Comput. Simulation 65 (1–2) (2004) 69–75.
[12] A. Alodah, O. Seidou, The adequacy of stochastically generated climate time series for water resources systems risk and performance assessment, Stoch. Environ. Res. Risk Assess. 33 (1) (2019) 253–269.
[13] J. Clarke, Energy Simulation in Building Design, Routledge, 2007.
[14] I. Hall, R. Prairie, H. Anderson, E. Boes, Generation of a Typical Meteorological Year, Tech. rep., Sandia Labs., Albuquerque, NM (USA), 1978.
[15] R. Festa, C.F. Ratto, Proposal of a numerical procedure to select reference years, Sol. Energy 50 (1) (1993) 9–17.
[16] M. Gazela, E. Mathioulakis, A new method for typical weather data selection to evaluate long-term performance of solar energy systems, Sol. Energy 70 (4) (2001) 339–348.
[17] F. Song, Q. Zhu, R. Wu, Y. Jiang, A. Xiong, B. Wang, Y. Zhu, Q. Li, Meteorological data set for building thermal environment analysis of China, 2007.

[18] P. Rastogi, On the Sensitivity of Buildings to Climate: the Interaction of Weather and Building Envelopes in Determining Future Building Energy Consumption, Tech. rep., EPFL, 2016.

[19] S. Farah, W. Saman, J. Boland, Development of robust meteorological year weather data, Renew. Energy 118 (2018) 343–350.

[20] P. Rastogi, M. Andersen, Embedding stochasticity in building simulation through synthetic weather files, in: Proceedings of BS 2015, IBPSA, 2015, pp. 963–970.

[21] T. Pesch, S. Schröders, H.-J. Allelein, J.-F. Hake, A new Markov-chain-related statistical approach for modelling synthetic wind power time series, New J. Phys. 17 (5) (2015) 055001.

[22] H. Nfaoui, H. Essiarab, A. Sayigh, A stochastic Markov chain model for simulating wind speed time series at Tangiers, Morocco, Renew. Energy 29 (8) (2004) 1407–1418.

[23] G. Papaefthymiou, B. Klockl, MCMC for wind power simulation, IEEE Trans. Energy Convers. 23 (1) (2008) 234–240.

[24] S. Kennedy, P. Rogers, A probabilistic model for simulating long-term wind-power output, Wind Eng. 27 (3) (2003) 167–181.

[25] D.C. Hill, D. McMillan, K.R. Bell, D. Infield, Application of auto-regressive models to UK wind speed data for power system impact studies, IEEE Trans. Sustain. Energy 3 (1) (2011) 134–141.

[26] Y. Ge, Y. Nan, L. Bai, A hybrid prediction model for solar radiation based on long short-term memory, empirical mode decomposition, and solar profiles for energy harvesting wireless sensor networks, Energies 12 (24) (2019) 4762.

[27] J. Ekström, M. Koivisto, I. Mellin, J. Millar, E. Saarijärvi, L. Haarla, Assessment of large scale wind power generation with new generation locations without measurement data, Renew. Energy 83 (2015) 362–374.

[28] J.M. Morales, R. Minguez, A.J. Conejo, A methodology to generate statistically dependent wind speed scenarios, Appl. Energy 87 (3) (2010) 843–855.

[29] D.D. Le, G. Gross, A. Berizzi, Probabilistic modeling of multisite wind farm production for scenario-based applications, IEEE Trans. Sustain. Energy 6 (3) (2015) 748–758.

[30] M.J. Holmes, J.N. Hacker, Climate change, thermal comfort and energy: Meeting the design challenges of the 21st century, Energy Build. 39 (7) (2007) 802–814.

[31] R. Barrett, E. Keeble, G. Levermore, T. Muneer, J. Page, C. Sanders, A. Wright, CIBSE guide j: Weather, solar and illuminance data, 2002.

[32] G.J. Levermore, J. Parkinson, Analyses and algorithms for new test reference years and design summer years for the UK, Build. Serv. Eng. Res. Technol. 27 (4) (2006) 311–325.

[33] T. CIBSE, Design summer years for London, the chartered institution of building services engineers London, 2014.

[34] M.E. Eames, An update of the UK's design summer years: Probabilistic design summer years for enhanced overheating risk analysis in building design, Build. Serv. Eng. Res. Technol. 37 (5) (2016) 503–522.

[35] M.F. Jentsch, M.E. Eames, G.J. Levermore, Generating near-extreme Summer Reference Years for building performance simulation, Build. Serv. Eng. Res. Technol. 36 (6) (2015) 701–727.

[36] K.K.-L. Lau, E.Y.-Y. Ng, P.-W. Chan, J.C.-K. Ho, Near-extreme summer meteorological data set for sub-tropical climates, Build. Serv. Eng. Res. Technol. 38 (2) (2017) 197–208.

[37] D. Ferrari, T. Lee, Beyond TMY: Climate data for specific applications, in: Proceedings 3rd International Solar Energy Society Conference–Asia Pacific Region, ISES-AP-08, 2008.

[38] D.B. Crawley, L.K. Lawrie, et al., Rethinking the TMY: is the 'typical'meteorological year best for building performance simulation, in: Conference: Building Simulation, 2015, pp. 2655–2662.

[39] M. Herrera, A.P. Ramallo-González, M. Eames, A.A. Ferreira, D.A. Coley, Creating extreme weather time series through a quantile regression ensemble, Environ. Model. Softw. 110 (2018) 28–37.

[40] V.M. Nik, Application of typical and extreme weather data sets in the hygrothermal simulation of building components for future climate–A case study for a wooden frame wall, Energy Build. 154 (2017) 30–45.

[41] G. Pernigotto, A. Prada, A. Gasparella, Extreme reference years for building energy performance simulation, J. Build. Perform. Simul. 13 (2) (2020) 152–166.

[42] S. Guo, D. Yan, T. Hong, C. Xiao, Y. Cui, A novel approach for selecting typical hot-year (THY) weather data, Appl. Energy 242 (2019) 1634–1648.

[43] H. Li, T. Zhang, A. Wang, M. Wang, J. Huang, Y. Hu, A new method of generating extreme building energy year and its application, Energy 278 (2023) 128020.

[44] W.-P. Schill, Residual load, renewable surplus generation and storage requirements in Germany, Energy Policy 73 (2014) 65–79.

[45] F. Trieb, A. Thess, Storage plants–a solution to the residual load challenge of the power sector? J. Energy Storage 31 (2020) 101626.

[46] T.H. Ruggles, K. Caldeira, Wind and solar generation may reduce the inter-annual variability of peak residual load in certain electricity systems, Appl. Energy 305 (2022) 117773.

[47] M. Ohba, Y. Kanno, S. Bando, Effects of meteorological and climatological factors on extremely high residual load and possible future changes, Renew. Sustain. Energy Rev. 175 (2023) 113188.

[48] Y. Scholz, L. von Bremen, G. Lohmann, W. Hu, M. Schroedter-Homscheidt, Dunkelflaute and long-term electric energy shortage events in Europe, 2023.

[49] F. Nitsch, Y. Scholz, W. Hu, K. von Krbek, R. Stegen, A.A. El Ghazi, U. Frey, K. Nienhaus, R. Finck, V. Slednev, et al., Versorgungsicherheit in deutschland und mitteleuropa während extremwetter-ereignissen (VERMEER)-der beitrag des transnationalen stromhandels bei hohen anteilen erneuerbarer energien, 2023.

[50] S. Höltinger, C. Mikovits, J. Schmidt, J. Baumgartner, B. Arheimer, G. Lindström, E. Wetterlund, The impact of climatic extreme events on the feasibility of fully renewable power systems: A case study for Sweden, Energy 178 (2019) 695–713.

[51] V. Slednev, Development of a Techno-Economic Energy System Model Considering the Highly Resolved Conversion and Multimodal Transmission of Energy Carriers on a Global Scale (Ph.D. thesis), Karlsruhe Institute of Technology, Karlsruhe, Germany, 2024, URL https://publikationen.bibliothek.kit.edu/1000170863.

[52] ENTSO-E, Ten-year network development plan 2022, 2022, (Accessed 10 December 2024). URL https://2022.entsos-tyndp-scenarios.eu/wp-content/uploads/2022/04/TYNDP2022_Joint_Scenario_Full-Report-April-2022.pdf.

[53] Y. Scholz, Renewable Energy Based Electricity Supply at Low Costs-Development of the REMix Model and Application for Europe (Ph.D. thesis), Universität Stuttgart, 2012.

[54] D. Stetter, Enhancement of the REMix Energy System Model: Global Renewable Energy Potentials, Optimized Power Plant Siting and Scenario Validation (Ph.D. thesis), Universtität Stuttgart, 2014.

[55] H. Hersbach, B. Bell, P. Berrisford, S. Hirahara, A. Horányi, J. Muñoz-Sabater, J. Nicolas, C. Peubey, R. Radu, D. Schepers, et al., The ERA5 global reanalysis, Q. J. R. Meteorol. Soc. 146 (730) (2020) 1999–2049.

[56] H.C. Gils, H. Gardian, M. Kittel, W.-P. Schill, A. Murmann, J. Launer, F. Gaumnitz, J. van Ouwerkerk, J. Mikurda, L. Torralba-Díaz, Model-related outcome differences in power system models with sector coupling—Quantification and drivers, Renew. Sustain. Energy Rev. 159 (2022) 112177.

[57] H. Gardian, H.C. Gils, M. Kittel, A. Murmann, J. Launer, F. Gaumnitz, A. Fehler, J. van Ouwerkerk, J. Mikurda, L. Torralba-Díaz, C. Krüger, T. Janßen, A. Zerrahn, Model input and output data of the FlexMex model comparison, 2024, https://zenodo.org/records/5802178, (Accessed 02 August 2024).

[58] M. Wetzel, E.S.A. Ruiz, F. Witte, J. Schmugge, S. Sasanpour, M. Yeligeti, F. Miorelli, J. Buschmann, K.-K. Cao, N. Wulff, et al., Remix: a gams-based framework for optimizing energy system models, Journal of Open Source Software 9 (99) (2024) 6330.

[59] ENTSO-E, Ten-year network development plan 2016, 2016, (Accessed 10 December 2024). URL https://eepublicdownloads.entsoe.eu/clean-documents/tyndp-documents/TYNDP%202016/rgips/TYNDP2016%20Scenario%20Development%20Report%20-%20Final.pdf.

[60] M. Kittel, W.-P. Schill, Measuring the Dunkelflaute: How (not) to analyze variable renewable energy shortage, Environ. Res.: Energy 1 (3) (2024) 035007.

[61] F. Mockert, C.M. Grams, T. Brown, F. Neumann, Meteorological conditions during periods of low wind speed and insolation in Germany: The role of weather regimes, Meteorol. Appl. 30 (4) (2023) e2141.

[62] I.R.E.A. (IRENA), Renewable Capacity Statistics 2023, International Renewable Energy Agency, Abu Dhabi, 2023, (Accessed 10 December 2024). URL https://www.irena.org/Publications/2023/Mar/Renewable-capacity-statistics-2023.

[63] A. Bagga, S. Sridhar, Z. Holman, B. Sergi, J. Osorio, M. Panwar, T. Lowder, R. Hovsapian, Impact of detailed parameter modeling of open-cycle gas turbines on production cost simulation, in: 2023 North American Power Symposium, NAPS, IEEE, 2023, pp. 1–6.

[64] C.A. Hunter, M.M. Penev, E.P. Reznicek, J. Eichman, N. Rustagi, S.F. Baldwin, Techno-economic analysis of long-duration energy storage and flexible power generation technologies to support high-variable renewable energy grids, Joule 5 (8) (2021) 2077–2101.

[65] H. Farhat, C. Salvini, Novel gas turbine challenges to support the clean energy transition, Energies 15 (15) (2022) 5474.

[66] K. Guerra, P. Haro, R. Gutiérrez, A. Gómez-Barea, Facing the high share of variable renewable energy in the power system: Flexibility and stability requirements, Appl. Energy 310 (2022) 118561.

[67] X. Wang, L. Duan, Peak regulation performance study of the gas turbine combined cycle based combined heating and power system with gas turbine interstage extraction gas method, Energy Convers. Manage. 269 (2022) 116103.

[68] N.A. Sepulveda, J.D. Jenkins, F.J. De Sisternes, R.K. Lester, The role of firm low-carbon electricity resources in deep decarbonization of power generation, Joule 2 (11) (2018) 2403–2420.

[69] N. Nguyen, J. Mitra, An investigation into the role of gas turbines in supporting renewable energy integration, in: 2018 North American Power Symposium, NAPS, IEEE, 2018, pp. 1–6.

[70] Fraunhofer Institute for Solar Energy Systems ISE, Levelized Cost of Electricity – Renewable Energy Technologies, Tech. rep., Fraunhofer ISE, Freiburg, Germany, 2024, (Accessed 22 July 2025). URL https://www.ise.fraunhofer.de/content/dam/ise/en/documents/publications/studies/EN2024_ISE_Study_Levelized_Cost_of_Electricity_Renewable_Energy_Technologies.pdf.

[71] D. Cui, S. Liang, D. Wang, Observed and projected changes in global climate zones based on Köppen climate classification, Wiley Interdiscip. Rev.: Clim. Chang. 12 (3) (2021) e701.

[72] K. Sudhakar, W. Ngui, I. Kirpichnikova, et al., Energy analysis of utility-scale PV plant in the rain-dominated tropical monsoon climates, Case Stud. Therm. Eng. 26 (2021) 101123.

[73] R. Geen, S. Bordoni, D.S. Battisti, K. Hui, Monsoons, ITCZs, and the concept of the global monsoon, Rev. Geophys. 58 (4) (2020) e2020RG000700.
[74] R. Evins, R. Alexandra, E. Wiebe, M. Wood, M. Eames, The impact of local variations in a temperate maritime climate on building energy use, J. Build. Perform. Simul. 13 (2) (2020) 167–181.
[75] A. Aszódi, B. Biró, L. Adorján, Á.C. Dobos, G. Illés, N.K. Tóth, D. Zagyi, Z.T. Zsiborás, Comparative analysis of national energy strategies of 19 European countries in light of the green deal's objectives, Energy Convers. Manag.: X 12 (2021) 100136.
[76] H. Jianchao, Z. Ruoyu, L. Pingkuo, Z. Lyuyang, A review and comparative analysis on energy transition in major industrialized countries, Int. J. Energy Res. 45 (2) (2021) 1246–1268.
[77] D. Kraal, R.J. Heffron, M. Hazrati, H. Hussein, A. Phillips, Energy policy distractions to renewable programs: a comparative assessment, Sustain. Earth Rev. 8 (1) (2025) 1–16.
[78] W. Hu, Y. Scholz, M. Yeligeti, Y. Deng, P. Jochem, Future electricity demand for Europe: Unraveling the dynamics of the Temperature Response Function, Appl. Energy 368 (2024) 123387.
[79] N. Mattsson, V. Verendel, F. Hedenus, L. Reichenberg, An autopilot for energy models–Automatic generation of renewable supply curves, hourly capacity factors and hourly synthetic electricity demand for arbitrary world regions, Energy Strat. Rev. 33 (2021) 100606.
[80] O. Miralles, D. Steinfeld, O. Martius, A.C. Davison, Downscaling of historical wind fields over Switzerland using generative adversarial networks, Artif. Intell. Earth Syst. 1 (4) (2022) e220018.
[81] W. Hu, Y. Scholz, M. Yeligeti, L. von Bremen, Y. Deng, Downscaling ERA5 wind speed data: a machine learning approach considering topographic influences, Environ. Res. Lett. 18 (9) (2023) 094007.
[82] J.C. Osorio-Aravena, A. Aghahosseini, D. Bogdanov, U. Caldera, N. Ghorbani, T.N.O. Mensah, J. Haas, E. Muñoz-Cerón, C. Breyer, Synergies of electrical and sectoral integration: Analysing geographical multi-node scenarios with sector coupling variations for a transition towards a fully renewables-based energy system, Energy 279 (2023) 128038.
[83] Y. Deng, K.-K. Cao, W. Hu, R. Stegen, K. von Krbek, R. Soria, P.R.R. Rochedo, P. Jochem, Harmonized and open energy dataset for modeling a highly renewable Brazilian power system, Sci. Data 10 (1) (2023) 103.
[84] A. Elkhatat, S.A. Al-Muhtaseb, Combined "renewable energy–thermal energy storage (RE–TES)" systems: a review, Energies 16 (11) (2023) 4471.
[85] F. Schipfer, E. Mäki, U. Schmieder, N. Lange, T. Schildhauer, C. Hennig, D. Thrän, Status of and expectations for flexible bioenergy to support resource efficiency and to accelerate the energy transition, Renew. Sustain. Energy Rev. 158 (2022) 112094.
[86] S. Shahzad, E. Jasińska, Renewable revolution: A review of strategic flexibility in future power systems, Sustainability 16 (13) (2024) 5454.
[87] Y. Li, K. Xie, L. Wang, Y. Xiang, Exploiting network topology optimization and demand side management to improve bulk power system resilience under windstorms, Electr. Power Syst. Res. 171 (2019) 127–140.
[88] Q. Zhang, J. Li, Demand response in electricity markets: A review, in: 2012 9th International Conference on the European Energy Market, IEEE, 2012, pp. 1–8.
[89] F. Wang, H. Xu, T. Xu, K. Li, M. Shafie-Khah, J.P. Catalão, The values of market-based demand response on improving power system reliability under extreme circumstances, Appl. Energy 193 (2017) 220–231.